PHOTOIONIZATION MASS SPECTROMETRY: A STUDY OF NO_2 AND NO

Thesis for the Degree of Ph. D.
MICHIGAN STATE UNIVERSITY
PAUL CHARLES KILLGOAR, JR.
1972

ABSTRACT

PHOTOIONIZATION MASS SPECTROMETRY:
A STUDY OF NO_2 AND NO

By

Paul Charles Killgoar, Jr.

The discrepancies among the reported values for the ionization potential of NO_2 led to a reinvestigation of this molecule by means of photoionization mass spectrometry. A careful study of the threshold region revealed considerable autoionization structure. The measured appearance potential of NO_2^+ is 9.62 eV, which combined with other data gives $9.25 \leq I.P.(NO_2) \leq 9.62$ eV. The results of this study suggest that the value is closer to the upper limit.

Fragmentation of NO_2 into NO^+ and O also was studied and the dependence of the dissociative lifetime of metastable NO_2^{+*} on the quantum state of its bending vibration was investigated.

The observed autoionization structure of the NO_2^+ photoionization efficiency curve has been assigned to Rydberg series converging to higher ionization potentials.

The photoionization efficiency curve of NO^+ was also obtained. Considerable fine structure was observed in the

threshold region (9.25-10.0 eV) which is attributed to vibrational autoionization. This fine structure has been assigned to Rydberg series converging to the excited vibrational levels of the ground NO^+ ion ($^1\Sigma^+$). The autoionization structure above threshold has been correlated with existing Rydberg series of the NO molecule.

PHOTOIONIZATION MASS SPECTROMETRY: A STUDY OF NO_2 AND NO

By

Paul Charles Killgoar, Jr.

A THESIS

Submitted to
Michigan State University
in partial fulfillment of the requirements
of the degree of

DOCTOR OF PHILOSOPHY

Department of Chemistry

1972

ACKNOWLEDGMENTS

I wish to express my sincere appreciation to Dr. George Leroi for his guidance and encouragement without which this work would never have been completed.

I also wish to thank Dr. Joseph Berkowitz and Dr. William Chupka of Argonne National Laboratory for allowing me access to their instrument, their patience with my mistakes and their sincere interest in my education.

I would like to thank the members of the Molecular Spectroscopy Group and Dr. Daniel O'Hare for their friendship and many stimulating discussions, scientific and other, in the course of this work.

Financial support from Michigan State University, the Office of Naval Research and the Associated Midwest Universities of Argonne "Thesis Parts" program is appreciated.

Finally, I wish to thank my wife for her patience and understanding during these past three years.

TABLE OF CONTENTS

LIST OF TABLES

LIST OF TABLES (Cont.)

LIST OF FIGURES

INTRODUCTION

A photoionization mass spectrometer is simply a mass spectrometer with the conventional electron bombardment ionization source replaced by the radiation emanating from a vacuum ultraviolet monochromator. This modification increases the versatility and precision of the instrument. One of the main advantages is the energy resolution available using a monochromator instead of the electron gun. In an ideal case the energy spread of an electron beam is approximately 0.1 eV, but with appropriate slits a monochromator can give an energy resolution of 0.01 eV.

A second advantage which is much more useful is the energy dependence of the photoionization cross section at threshold. Wigner and others [1-3] have shown that the threshold law for direct ionization is

$$E^{n-1} \alpha \text{ cross section}, \qquad (1)$$

where n is the number of electrons leaving the collision complex. It is obvious that for electron impact the cross section is linear with energy; that is, the cross section rises very slowly from the baseline. This makes it very difficult to determine exactly where the onset actually occurs. For photon impact there is no energy dependence.

That means at the threshold the cross section ideally rises to some maximum value, after which it should vary very slowly with increasing energy, until the next threshold. This makes it much easier to determine the onset for ionization (the appearance potential).

The photoionization cross section is defined as the number of ions produced per photon absorbed

$$\sigma_i = \sigma N_i/(I_0 - I), \qquad (2)$$

where σ_i is the photoionization cross section, σ is the absorption cross section, N_i is the number of ions produced per second, I is the transmitted photon intensity and I_0 is the incident photon intensity. To measure this quantity with a single beam instrument is very difficult since I and I_0 cannot be measured simultaneously. To circumvent this, a quantity called the photoionization efficiency (P.I.E) is used instead. This is the number of ions produced per photon transmitted

$$\text{P.I.E.} = N_i/I \quad . \qquad (3)$$

It can be shown [4] that for absorptions of less than 10% of the total incident beam the ratio of the photoionization cross section to the photoionization efficiency is nearly unity.

At the outset, this research project involved the design and construction of a photoionization mass spectrometer. This instrument was to consist of a one-meter off-plane

Eagle mount vacuum ultraviolet monochromator coupled to a quadrupole mass spectrometer, each of which had been initially designed and constructed at the Frick Chemical Laboratory at Princeton University. One major difficulty encountered with this instrument was the limited flexibility of the vacuum ultraviolet monochromator. In the off-plane Eagle design the entrance and exit slits are located symmetrically above and below the Rowland circle [5]. When the instrument was initially designed the distance between the centers of the entrance and exit slits was only one inch. This distance was increased to four inches by modifying the front plate of the monochromator. Even with this adjustment, however, there was insufficient room to attach the quadrupole mass spectrometer to the monochromator and still have enough room remaining to couple a light source to the entrance slit.

It thus appeared that the experimental research which was to be the foundation of this dissertation would have to be significantly delayed while the photoionization instrument at Michigan State was extensively redesigned and constructed. In light of this tenuous future, a better instrument was sought, and the main portion of the experimental work described in this thesis was performed at the Argonne National Laboratory with the cooperation and guidance of Drs. Joseph Berkowitz and William Chupka of the Physics Division.

Initially the experimental portion of the research was to include a determination of the ionization potential of NO_2, for which a wide dispartiy existed in the reported values. It was hoped that a new investigation by various independent techniques would yield a consistent value. The methods to be used included ion-molecule reactions, fragmentation by photon-impact, and direct ionization of the NO_2 molecule itself. The ion-molecule reaction chosen was that between NO^+ and NO_2. Possible choices for the fragmentation experiments were CH_3NO_2 and nitric acid. The criterion used in choosing molecules for the fragmentation experiments was that the fragmentation into NO_2^+ upon photon impact was likely to be the first process. This point was important because to determine an accurate ionization potential from a fragmentation process an accurate appearance potential for the fragment of interest is necessary. Thus if the fragment is not formed as the first process it will have to compete with the primary fragmentation process, and its observed appearance potential will be somewhat higher than the true value. To complete this study of the NO_2 molecule, the fragmentation into NO^+ and O was investigated in detail, including the study of a metastable fragmentation. A Rydberg analysis of the autoionization structure was also performed.

During the performance of the various experiments a photoionization efficiency curve of NO^+ was obtained. Careful examination of the threshold region revealed some

unusual structure. The molecule NO has been well studied; however, no interpretation has been put forward for the structure (indeed it has only been mentioned once in the open literature). This fine structure has been interpreted in terms of Rydberg series converging to excited vibrational levels of the ground ionic state. The autoionization structure above threshold has been correlated with existing Rydberg series of the NO molecule.

EXPERIMENTAL

The Instrument

The photoionization efficiency data reported in this work were obtained using the one meter instrument at the Argonne National Laboratory [6,7]. This consisted of a one meter vacuum ultraviolet monochromator built by McPherson Instrument Co. (a modified Model 225) coupled to a 60^{0} magnetic-sector mass spectrometer as illustrated in Figure 1. The light sources employed were the hydrogen many-lined source generated by a continuous d.c. discharge and the continua of argon and helium, which were produced by a pulsed d.c. discharge. These lamps provided a range of photon energies from 9.0 to 20.7 eV (1300 Å - 600 Å). In order to utilize the higher energy photons (above 11 eV) the lamp was run windowless. To do this three stages of differential pumping were employed, in which the third stage was a pump on the monochromator chamber. With the argon source a typical operating pressure within the lamp was 150 torr and in the monochromator the pressure was maintained at or below 10^{-5} torr by the differential pumping.

The grating used in these experiments had 1200 lines/mm and a dispersion of 8.3 Å/mm. Entrance and exit slits of

Figure 1. The photoionization mass spectrometer.

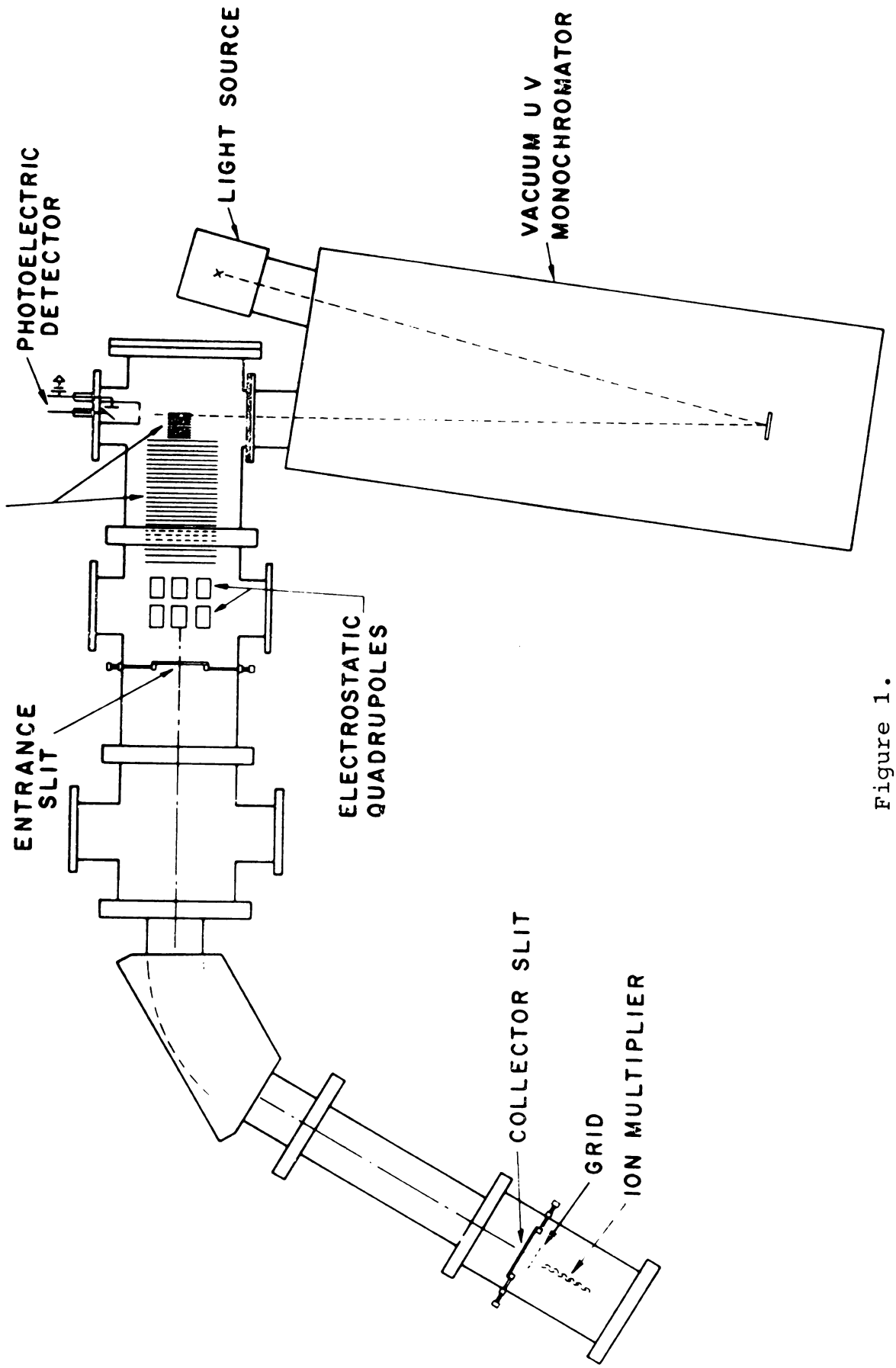
ION ACCELERATING PLATES
PHOTOELECTRIC DETECTOR
LIGHT SOURCE
VACUUM U V MONOCHROMATOR
ENTRANCE SLIT
ELECTROSTATIC QUADRUPOLES
COLLECTOR SLIT
GRID
ION MULTIPLIER

Figure 1.

300, 100 and 50 microns were used, depending on the conditions of a given experiment. With 100 micron slits the energy resolution in the wavelength region of interest (1300-600 Å) was approximately 0.01 eV.

The transmitted photon beam was detected by two different techniques. Initially a sodium salicylate phosphor deposited on a Pyrex window was employed; this was optically coupled to an R.C.A. 8850 photomultiplier by means of a lucite light pipe. Dow-Corning silicone grease was used to make the optical couplings between the light pipe and the Pyrex widnow and the light pipe and the face of the photomultiplier. Because the index of refraction of the grease is not very different from that of the Pyrex window, the lucite light pipe and the window of the photomultiplier, it reduces the loss of light by scattering at the surfaces. It became evident that the chemicals being used in these experiments had a deteriorating effect on the quality of the phosphor, eventually leading to non-linearities in the photon detection. This problem was not immediately diagnosed and therefore much of the data had to be re-run using the second method of photon detection, a bare nickel photocathode. The nickel surfaces were polished so as to increase the efficiency of the detector. The principle involved in this method of detection was as follows: a photon of energy $h\nu$, which is greater in energy than the work function of nickel (5.01 eV) hits the nickel surface ejecting a photoelectron which is then collected by a

second nickel plate kept at a constant positive 45 volts potential relative to the first plate. Whereas the phosphor has a linear efficiency in the photon range of interest [8] the nickel photocathode does not [9]. A calibration curve, obtained by comparing the efficiency of the nickel detector to that of a newly prepared phosphor, was used to correct the experimental data. The current signal generated by either the photomultiplier or the nickel detector was then measured by a vibrating reed electrometer. This signal was then fed simultaneously into a strip chart recorder, for monitoring purposes, and into a voltage to frequency converter. This encoded signal was then fed into one half of a dual scalar and then placed on magnetic tape.

When the photon beam passed through the sample gas, ions were produced which were pushed out of the ionization chamber by means of a repeller voltage into the region denoted by the ion accelerating plates in Figure 1. These plates were used to accelerate the ions to an appropriate potential for separation of the masses; in these experiments this potential was approximately 4 KV. The ions then entered the region of the electrostatic quadrupole lens system. The function of this lens system was to focus the ion beam into a line image before entering the entrance slit of the mass spectrometer. The ions then drifted through a field-free region into the magnetic field region where the masses were separated and the mass of interest focused on to the ion detector. Ion detection was accomplished by

means of a bare 20 stage electron multiplier. The signal was taken off the multiplier by two methods simultaneously. The first method utilized pulse counting techniques; this was accomplished by counting the positive pulses generated at the last dynode of the electron multiplier [10]. These pulses were amplified and fed into the other half of the dual scalar to be counted and placed on the magnetic tape. The second technique involved measuring the current produced at the anode by means of a second vibrating reed electrometer. This signal was then put on the strip chart recorder, again for purposes of monitoring the ion signal. The photon energy was selected by means of a stepping motor coupled directly to the monochromator drive. The process of collecting the data was essentially completely automated. In an experiment the stepping motor stepped to a selected wavelength, a preset counter received a start pulse and counted an external clock which put out one pulse every one-tenth of a second. The number of pulses counted thus determined the duration of data collection. After the preset time the scalars stopped counting, the stepping motor advanced the monochromator drive, the data in the scalars was placed on the magnetic tape, the scalars were cleared, and the process repeated.

The Ionization of NO_2

The NO_2 used in these experiments was obtained from the Matheson Company, Inc. and had a stated purity of

99.95%. The gas sample was found to contain a significant amount of NO impurity, however, as much as 5-10%. Experiments were performed using 50 and 100 micron slits. The 100 micron slits were employed in the threshold region (1300 - 1100 Å) because of the extremely low photoionization cross section encountered there. T. Nakayama, et al. [11] reported an ionization cross section of 10^{-20} cm^2 in this region. The remainder of the data (1100 - 600 Å) were taken with the higher resolution afforded by the 50 micron slits. With the 100 micron slits data were collected every 0.25 Å and the monochromator was stepped in 0.20 Å increments when the 50 micron slits were used. The sample gas was allowed to enter the sample cell through a metal and teflon gas handling line, and the sample pressure in the cell was controlled by means of a stainless steel micrometer valve. The pressure of the sample was monitored by measuring the pressure of the gas in the ionization region by means of an ionization gauge. When the pressure in this region was 10^{-5} torr it was estimated that the pressure in the sample cell was 10^{-2} to 10^{-3} torr, based on the specified pumping speed of the system. No actual measurements of the pressure in the cell were made, however. The cylinder of NO_2 was inverted so that the sample was taken directly from the liquid phase [12].

Initially the data were taken at room temperature; however, in order to minimize the contribution of hot band structure to the photoionization efficiency curve a cold

cell was employed. The cell was designed and built at Argonne National Laboratory and is represented schematically in Figure 2. Cooling was accomplished by passing a stream of dry nitrogen gas through a coiled copper tube which was submerged in liquid nitrogen. The cooled gas then passed through the tube represented in Figure 2, thus cooling the walls of the cell. The sample gas was forced to take a circuitous route to the region of the beam by means of baffles, thereby increasing the efficiency of the cooling. The temperature attained in the cell was controlled by varying the flow rate of the dry nitrogen through the cooling coil, and monitored by means of an iron/constantan thermocouple. The normal operating temperature for the system when using NO_2 as the sample gas was approximately -35^0. It should be noted that NO_2 did not condense until -73^0 at the operating pressures of these experiments. It was determined that at temperatures near the condensation point the formation of the dimer, N_2O_4, became a distinct possibility. Therefore to reduce the possibility of detecting NO_2 from a process involving N_2O_4 the relatively higher operating temperature was chosen.

Initially in these experiments the data were taken using the sodium salicylate phosphor detector, but the NO_2 seriously affected the detector efficiency with time. Once this problem was diagnosed the remaining data were taken with a nickel photocathode detector. The helium gas used in the lamp was passed through an activated charcoal trap

Figure 2. Schematic drawing of the cold cell.

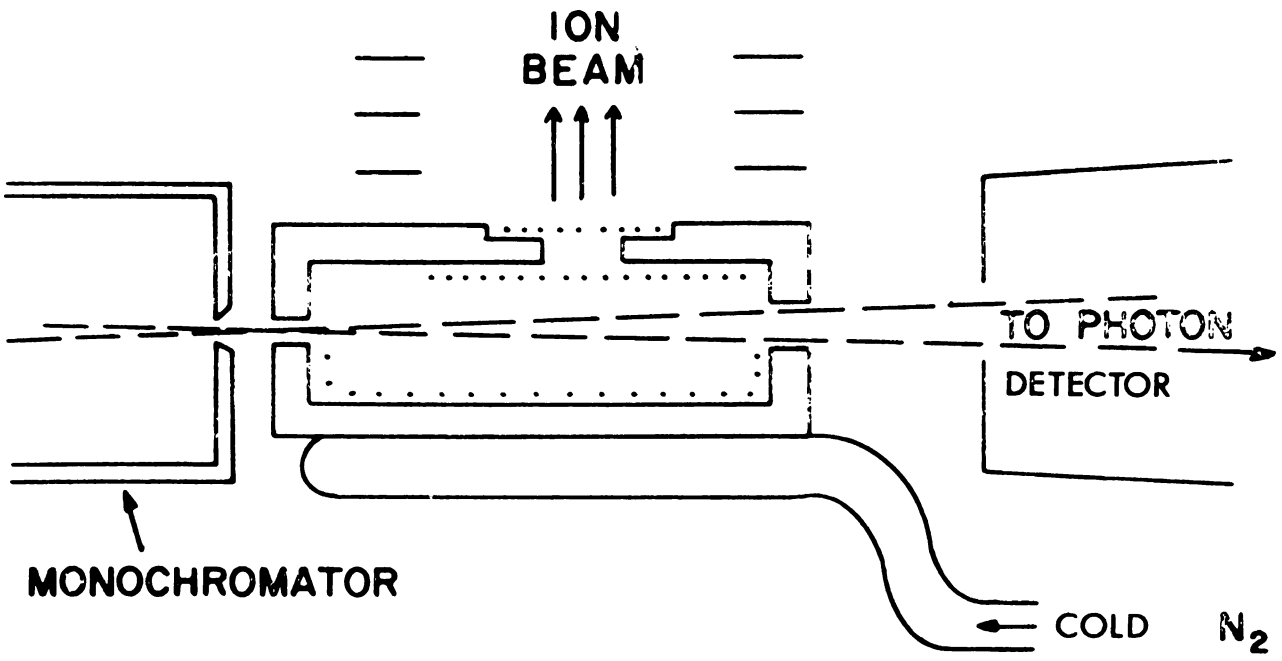

(top view)

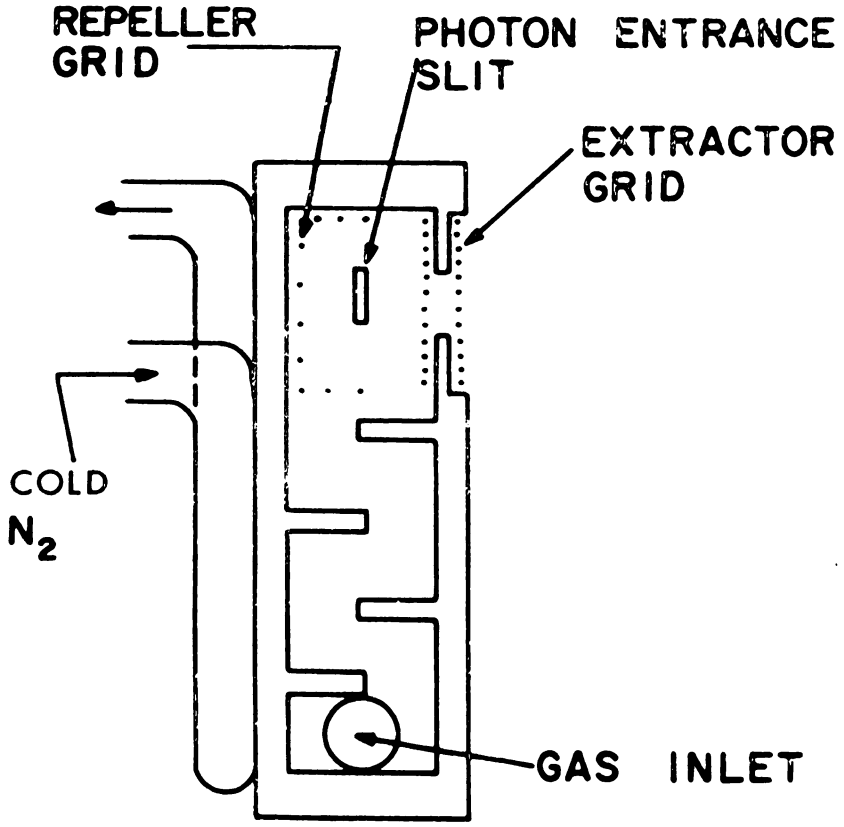

(end view)

Figure 2.

which was submerged in liquid nitrogen in order to remove any impurities and thus remove extraneous lines from the helium spectrum. Argon was used directly from the cylinder and had a claimed purity of 99.995%.

A special experiment was performed in the region 1300 - 1285 Å. The objective of this experiment was to carefully determine if any structure was present below 9.62 eV (1289 Å), and indeed whether the peak observed in previous experiments at 9.62 eV was real. In this experiment data were collected every 0.25 Å for ten minutes using 100 micron slits. Because of the low cross sections observed in this region it was hoped that the statistics would be improved by the long counting times.

The Fragmentation of NO_2

The same sample cell employed in the ionization experiments was used to study the fragmentation of NO_2. The significant problem encountered in measuring the NO^+ production from NO_2 was the presence of NO impurity from the decomposition of the sample in the cylinder. Initially the cylinder was inverted as suggested by Brundle [12], but even under these conditions the NO impurity was still significant, (~5%). In an attempt to reduce this impurity level a different technique was employed. A liquid NO_2 sample was transferred to a teflon container equipped with a teflon valve. The flask was connected directly to the gas inlet of the sample cell with teflon tubing, thus

eliminating the metal gas line. It was felt that by removing as much metal as possible any surface decomposition might be minimized. The flask was submerged in an ice/H_2O temperature bath to help regulate the pressure of the sample because the teflon valve was a relatively insensitive flow regulator. Before taking any data the sample was pumped for approximately one hour in an attempt to remove the NO. Even with all these precautions the NO impurity level was not significantly reduced below the 5% level [13].

All the fragmentation data were taken with the helium lamp, 100 micron slits, and the nickel photocathode detector.

Ion-Molecule Reaction of NO^+ with NO_2

To perform the collision experiment between NO^+ and NO_2 a different cell was employed, as well as a different electronics package. The sample cell used in these experiments consisted of two chambers instead of the conventional single-chamber source. This source is represented schematically in Figure 3. In these experiments NO gas was photoionized and accelerated to have varying amounts of kinetic energy before being allowed to collied with the NO_2. If one monitors the production of NO_2^+ as a function of the collision energy and the internal energy of the NO^+ ion, the ionization potential of NO_2 may be determined in principle. To perform the experiment NO gas was allowed to enter the ionization chamber of the source, the monochromator was set at a specific wavelength of sufficient

Figure 3. The collision source.

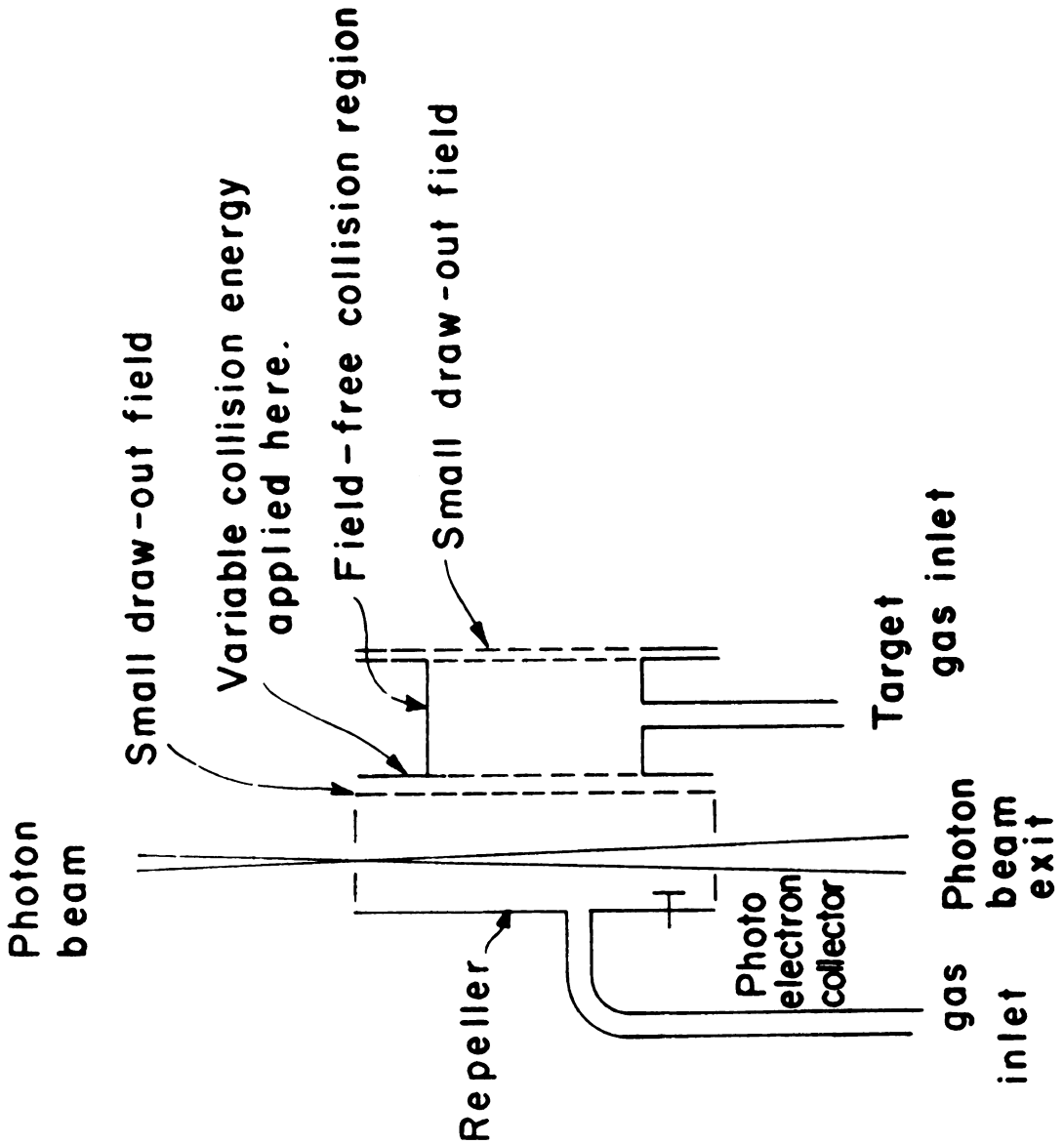
Photon beam
Small draw-out field
Variable collision energy applied here.
Field-free collision region
Small draw-out field
Target gas inlet
Photon beam exit
Photo electron collector
Repeller
gas inlet

Figure 3.

energy to just ionize the NO gas (9.25 eV), i.e. to produce NO^+ in the ground vibrational and electronic state, and NO_2 gas was allowed into the second chamber where it was available for collisions with the NO^+. The NO^+ ions had been accelerated by means of a potential applied to an extractor plate. In doing these experiments the total pressure of the sample was about 10^{-5} torr in the ionization region, composed of approximately equal amounts of NO and NO_2.

Data were taken with a multichannel analyzer coupled to a staircase voltage (a step voltage of controllable height and duration). The collision energy was determined by the ramp voltage. The multichannel analyzer collected and stored the data; then the voltage was increased by the ramp and the data collected and stored in the next channel, etc. In these experiments 200 channels were utilized and to help eliminate spurious effects, such as might occur with pressure changes, data were collected in each channel for one tenth of a second with multiple scans across the 200 channels. Data were collected in these experiments continuously for several hours because of the short counting duration in each channel and the expected small cross section for the process. The total range of accelerating voltage was approximately 5 volts. Thus with the 200 channels used this amounted to 0.025 volts per channel.

The NO sample was taken without further purification directly from the cylinder supplied by the Matheson Company, Inc., and had a stated purity of 98.5%. The NO_2 used was

the same as described previously.

Fragmentation of Nitric Acid and Nitromethane

To perform these experiments the collision ionization source was used (see Figure 3). In these experiments, however, no second gas was put into the second chamber. The sample of nitric acid was made up of a mixture of fuming nitric acid and concentrated sulfuric acid (50-50 by volume). The presence of the sulfuric acid was helpful in drying the nitric acid and thus reducing the concentration of water vapor. The sample was kept cold by means of an ice/H_2O temperature bath for purposes of reducing the vapor pressure of the sulfuric acid and increasing the relative vapor pressure of the nitric acid. The sample was contained in the same teflon cell described earlier. The gaseous nitric acid has a very adverse effect on the sodium salicylate phosphor, so data were collected using the nickel photocathode. For these experiments 300 micron slits were utilized and data were collected for the parent ion and the fragment NO_2^+ ion at 1 Å intervals.

The nitromethane fragmentation was done in the same cell as the nitric acid experiments, again using 300 micron slits and collecting data every Angstrom. The sample consisted of analytical reagent grade nitromethane liquid, contained in a glass tube. The vapor was allowed to enter the cell through the metal and glass gas handling system.

The Direct Ionization of NO

The NO sample used in these experiments was the same as described in the previous section on the ion-molecule experiments. The cold source used during these experiments was the same as that represented in Figure 2, and the temperature maintained for these experiments was approximately -135^{0}. In the threshold region (1350 - 1200 Å) data were collected with 50 and 100 micron slits, with the remainder of the data being taken with 100 micron slits (1200 - 600 Å). Again all the data were collected using the nickel photocathode detector.

THE IONIZATION AND FRAGMENTATION OF NO_2

Introduction

Nitrogen dioxide (NO_2) has been of interest, both experimentally and theoretically, for many years. Stimulated by the concern generated by the space effort and the ramifications of atmospheric molecules on pollution, this interest has persisted and indeed has recently increased.

The number of investigations of the ionization potential of NO_2 in the last forty years stands as a good example of this interest. Various approaches to obtain this value have been employed; spectroscopic [14,15], electron-impact [16-20], photoelectron spectroscopy [12,21,22], and photoionization with [23-25] and without mass analysis [11]. The results of these studies are summarized in Table I. As can be seen from the Table, the values vary over a wide range, well outside the expected accuracies of the methods employed. It was therefore one of the principle purposes of this investigation to obtain the best possible value of the ionization potential of this molecule.

The Ionization Potential of NO_2

It is known theoretically [26,27] and experimentally [28,29] that NO_2 is bent in its ground electronic state.

Table I. Reported first ionization potentials of NO_2.

Value (eV)	Technique	Reference
13.98 ± 0.12	Electron Impact	16
12.3 ± 0.2	Spectroscopic	14
12.07	Spectroscopic	15
11.3 ± 0.4	Photoionization[c]	25
11.27 ± 0.17	Electron Impact	19
11.25	Photoelectron[a]	22
11.0 ± 1	Electron Impact	20
10.2	Electron Impact	18
10.0	Photoelectron	12
9.91	Electron Impact[b]	17
9.8	Photoionization[c]	24
9.76	Photoionization	11
9.75 ± 0.01	Photoionization[c]	23
8.8	Photoelectron[d]	21

[a]Reported as vertical ionization potential.

[b]Determined from appearance potential of NO_2^+ from nitromethane.

[c]With mass analysis.

[d]Obtained using retarding field potential analyzer rather than energy selector analyzer of other P.E. workers.

Since NO_2 has one more electron than the linear CO_2 molecule, with the knowledge of the ground state configuration of CO_2 and the help of a correlation table [30] the ground state configuration of NO_2 can be predicted. Considering only the 17 valence shell electrons, the corresponding configurations are:

$$\begin{array}{lcccccccc} CO_2\ (180^0) & (\sigma_g)^2 & (\sigma_u)^2 & (\sigma_g)^2 & (\sigma_u)^2 & (\pi_u)^4 & (\pi_g)^4 & (\pi_u)^0 \\ & \downarrow & \downarrow & \downarrow & \downarrow & \downarrow & \downarrow & \downarrow & \downarrow \\ NO_2(134^0) & (1a_1)^2 & (1b_2)^2 & (2a_1)^2 & (2b_2)^2 & (1b_1)^2 & (3a_1)^2 & (1a_2)_2 & (3b_2)^2 & (4a_1)^1 \end{array}$$

It is the presence of the extra electron in the $4a_1$ orbital which contributes most to the change in geometry. Walsh [27] has discussed the influence of the different orbitals on the geometry of XY_2 molecules, and as may be seen from the appropriate Walsh diagram (Figure 4), it is the $4a_1$ orbital which is most stabilized by the departure from linearity. The first ionization of NO_2 results from the removal of this $4a_1$ electron, thus leaving a linear ion isoelectronic with CO_2.

In order to accurately determine the adiabatic ionization potential of a molecule by means of photon interaction techniques it must be possible to populate the ground vibrational level (all vibrational quantum numbers equal zero) of the ion. However, in the case of NO_2 the difference in geometry between the neutral molecule and the ion is so drastic that it is virtually impossible to populate the $v' = 0$ level of the bending vibration of the NO_2^+ ion

Figure 4. Walsh diagram for an XY_2 molecule.

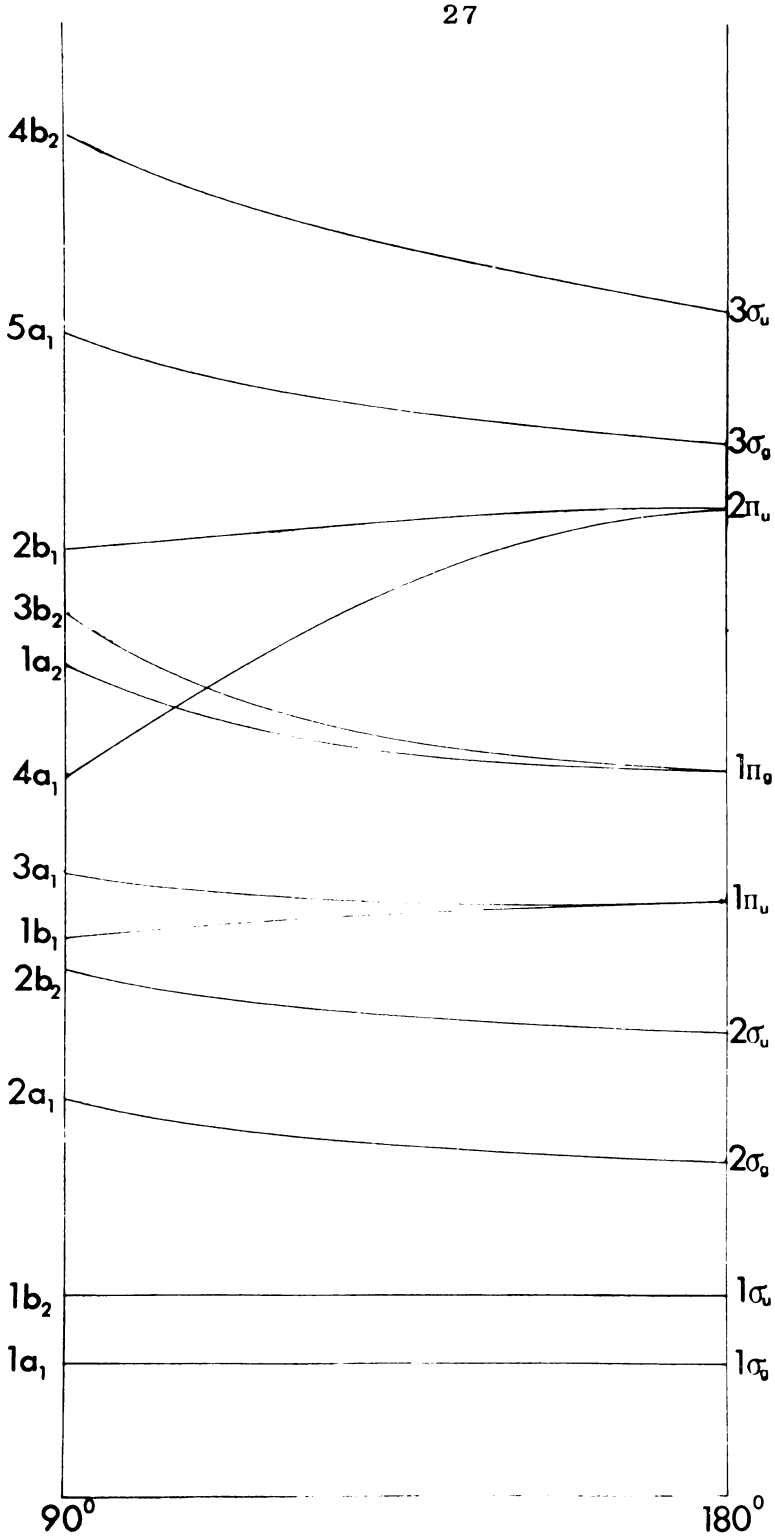
4b2
5a1
2b1
3b2
1a2
4a1
3a1
1b1
2b2
2a1
1b2
1a1
3σu
3σg
2πu
1πg
1πu
2σu
2σg
1σu
1σg
90°
180°

Figure 4.

directly. There is, however, an indirect method by which one still may accurately determine the adiabatic ionization potential, and that is to populate the lower vibrational levels of the ion by means of autoionization. This process relies upon the existence of another electronic state, usually a Rydberg level of the neutral molecule which converges to a higher ionization potential, overlapping the ionization continuum of interest. Essentially what is involved is the interaction of a discrete state with the ionization continuum of some electronic state. If a transition is made to the discrete state a radiationless transition (autoionization) to the continuum can occur. The Franck-Condon factors coupling the discrete to the continuous states also play an important role in the transition probability [31]. The total transition probability to the ionic state from the ground state then depends on two Franck-Condon factors instead of just one. There are three different types of autoionization, the two important forms being electronic and vibrational and a less important type being rotational [32]. The most commonly observed autoionization structure is attributed to electronic autoionization. Rydberg states converging to excited states of the molecular ion involve an excited ion core and a Rydberg electron. When the Rydberg electron is in the vicinity of the core electronic autoionization may occur resulting in the ejection of an electron and a decrease in the electronic energy of the core. The perturbation which accounts for the

mixing of the Rydberg state with the ionization continuum is a configuration interaction [33,34]. The second form of autoionization may occur when the discrete state is a vibrationally excited Rydberg state. That is, the electronic state of the ion core of the Rydberg level is the same as the electronic state of the ion to which the neutral molecule autoionizes; however, the core has some vibrational excitation. This excitation is then transferred to the Rydberg electron and the state makes the transition into the ionization continuum. The perturbation which is responsible for the mixing of states in this case results in the breakdown of the Born-Oppenheimer approximation [31,35].

Autoionization structure is usually exhibited as a peak or series of peaks superimposed upon the ionization continuum. However, this need not be the case. Fano [33] has discussed line shapes due to autoionization and has shown that it is possible to have a valley or "window resonance" in the ionization continuum.

The threshold region of the photoionization efficiency curve of NO_2^+ is shown in Figure 5. As can be seen there is a significant amount of structure, all of which must be attributed to autoionization of Rydberg levels.

Two vacuum ultraviolet absorption measurements in this region show the existence of one member ($n = 3$) of a Rydberg series converging to 12.86 eV. Nakayama, et al. [11] and Tanaka and Jursa [15] have shown that this state has vibrational structure with an average spacing of 640 cm^{-1}. The

Figure 5. Threshold region of NO_2^+ photoionization efficiency curve.

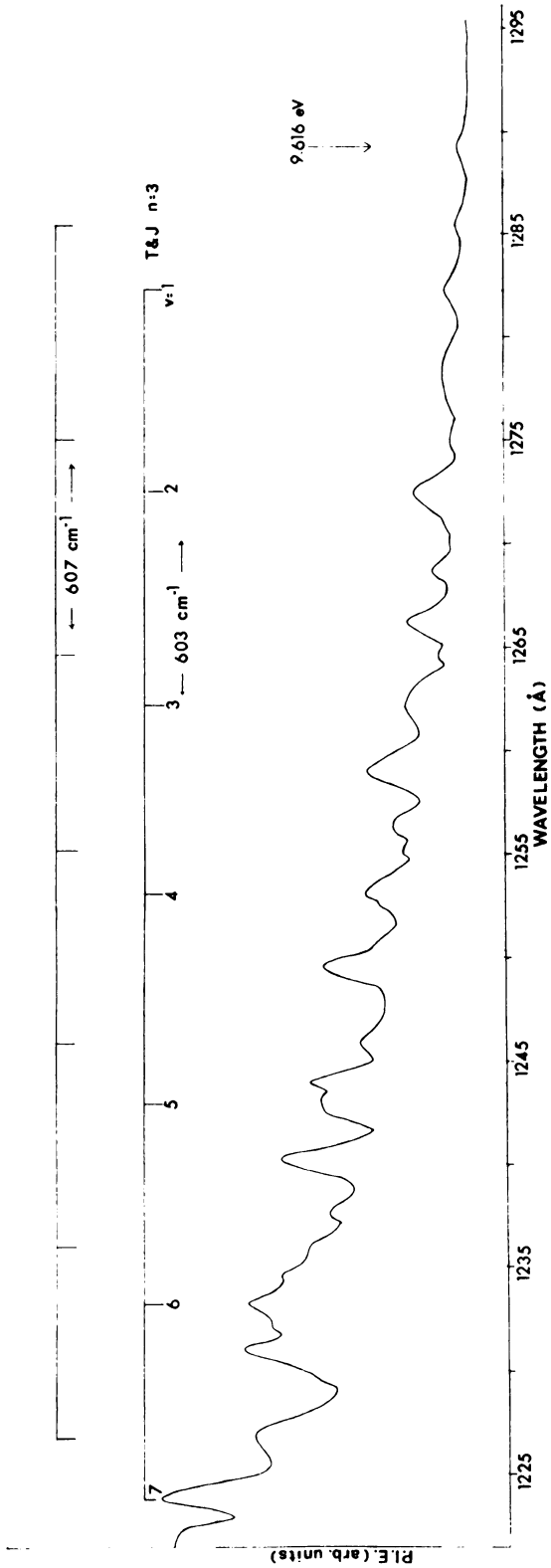
← 605 cm⁻¹ →
← 607 cm⁻¹ →
T&J n=3
v=1
← 603 cm⁻¹ →
9.616 eV
P.L.E. (arb. units)
WAVELENGTH (Å)
1225
1235
1245
1255
1265
1275
1285
1295
2
3
4
5
6
7

Figure 5.

vibrational spacing is assigned to the ν_2 bending vibration of NO_2^* (electronically excited NO_2). This member of the series has been observed to autoionize in the photoionization efficiency curve and is identified as T & J n = 3 in Figure 5. The observed vibrational spacing in the present case is 603 ± 50 cm^{-1}, which is within the experimental error of the measurements. Table II compares the peaks observed by Tanaka and Jursa with those of this experiment. It may be noted that the transition to v' = 0 reported to be at 1293 Å by Tanaka and Jursa was not observed in these experiments. To scan this region more carefully a special experiment was performed utilizing 10 minute counting times per point. Again no peak at 1293 Å could be detected. Since it was observed optically it is not immediately obvious why this transition is not observed in the photoionization efficiency curve. There are two different rationalizations for this phenomenon.

The first interpretation is the obvious conclusion that the v' = 0 level of this Rydberg state is below the adiabatic ionization potential of the NO_2 molecule. If this is the case, the v' = 0 level does not overlap the ionization continuum in any way and therefore no structure will be observed. This is not, however, the only interpretation. Even if the v' = 0 level is above the adiabatic ionization potential of the molecule, the Franck-Condon overlap of this level with the ionization continuum may be so small that the autoionization transition rate is too

Table II. Comparison of optically observed peaks to observed autoionization peaks.

V'	Tanaka and Jursa[a] (Å)	Intensity[a]	This Work Å
0	1292.8	6	----
1	1282.8	9	1282.30
2	1272.2	8	1272.80
3	1261.6	4	1262.50
4	1251.3	1	1253.55
5			1243.43
6			1234.30

[a]See reference 15.

small to be observed. There is a strong likelihood that this is really what is happening in the present case.

The Rydberg series in question has been assigned by Edquist, et al. [22] as one converging to the first excited ionic state at 12.86 eV. This excited state has been attributed to the removal of a $3b_2$ electron from NO_2. Upon examination of the Walsh diagram (Figure 4) it can be seen that the $3b_2$ electron stabilizes the linear configuration of the molecule. Removal of this electron should result in the excited electronic state of the NO_2^+ ion being more bent than the ground state of the molecule because of the increased influence of the $4a_1$ electron.

Rydberg levels are expected to exhibit the same vibrational structure as the state to which they converge, this being especially true of the higher members of a series [32]. It is therefore probable that the $n = 3$ member of the Rydberg series converging to 12.86 eV is at least as bent as the ground state of the molecule. This point is borne out by the fact that intensity measurements by Tanaka and Jursa (see Table II) show the $v' = 0,1,2$ and 3 levels to be about equal in intensity, thus indicating that the Franck-Condon factors are favorable for the optical transitions. For this reason, the vibrational ground state of this Rydberg level is unlikely to overlap the ionic ground state very much more than the molecular ground state does. These points are illustrated schematically in Figure 6.

Figure 6. Schematic representation for the autoionization structure in the threshold region of NO_2.

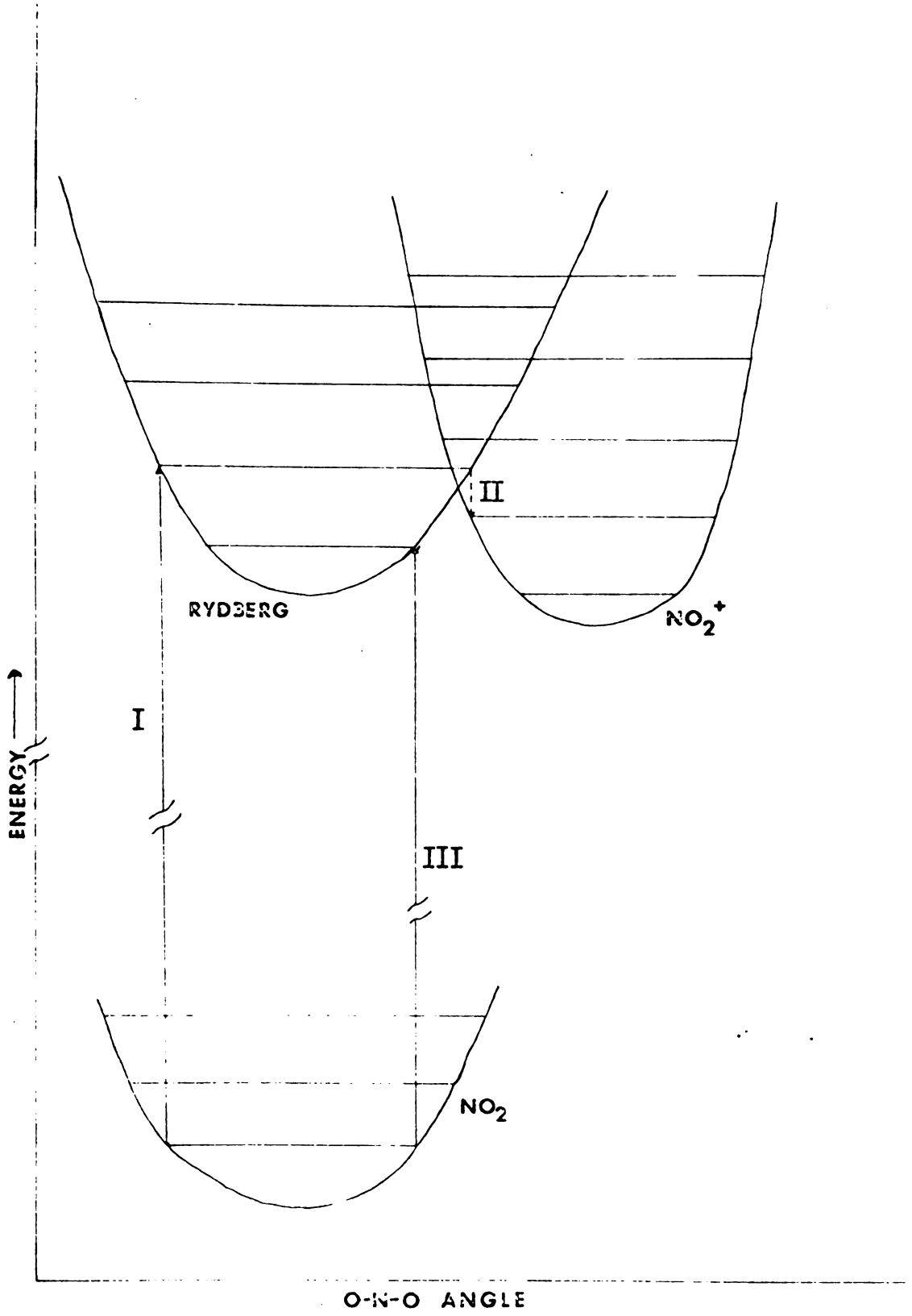

Figure 6.

If a transition is made from the molecular ground state to a Rydberg level with similar geometry, such as that denoted by I in Figure 6, the molecule may make the transition, denoted by II in Figure 6, into the ground ionic state. If this occurs a peak will be observed in the photoionization efficiency curve at the energy corresponding to transition I. If on the other hand a transition is made from the molecular ground state to the Rydberg level denoted by III, there is no way that this level can make a transition into the ionic state, except possibly by a tunneling process. If tunneling does occur the cross section for the process is so small it cannot be detected in these experiments.

It seems likely that this is the best explanation for the absence of the peak at 1293 Å. However, even with the above arguments for the unfavorable Franck-Condon factors for the autoionization transition one cannot exclude the possibility that the 1293 Å level is lower than the adiabatic ionization potential.

In Figure 5 two other vibrational progressions with the same average spacing can be seen in the 1300 - 1230 Å region. The assignment of these progressions is not immediately clear. It may be that these progressions are converging to the same excited state of the NO_2^+ ion as the progression identified by Tanaka and Jursa [15]. One argument against this possibility is the complete absence of any similar structure in the next member of the Rydberg

series; that is, only one progression is seen in this region. Another possible explanation for the existence of these progressions is that they can be due to vibrational autoionization of Rydberg series converging to vibrationally excited states of the ground electronic state of the ion. Although this is a good possibility, it remains unprovable at present. The possibility that these peaks are due to vibrational hot band structure can almost certainly be ruled out, because the structure did not diminish when the gas was cooled in some experiments. At the temperature of these experiments only $\sim 2\%$ of the molecules are expected to be in vibrationally excited states, and with the low cross sections observed this will never be an important contribution. As far as evaluation of the ionization potential is concerned, however, these progressions are of little relevance.

The lowest observable ion current due to photoionization occurs at 9.62 ± 0.01 eV (1288.8 Å). From the spectra in Figure 5, one predicts that the next peak at longer wavelength should occur at 1293 Å, and this is not seen. Therefore, from this investigation it appears that the ionization potential of NO_2 cannot be any greater than 9.62 ± 0.01 eV. This value is lower than any of the previous investigations made using photoionization techniques, and lower than all other reported values except one, that being 8.8 eV from the photoelectron investigations by Natalis and co-workers [21,36]. The higher sensitivity of

the instrument employed in this work accounts for the discrepancy between this result and the other photoionization results; however, it is difficult to explain why the photoelectron result of Natalis, et al. [21,36] is so much lower, and indeed, so much lower than the value obtained by other photoelectron experiments. In Natalis' photoelectron work resonance lines of Ar (1048 - 1067 Å) were used as the excitation source. In order for the photoelectron result to yield a value lower than the photoionization measurements, the exciting line must coincide with an autoionizing level which can populate the $v' = 0$ level of the ionic ground state. Upon examination of the photoionization efficiency curve in the region of the 1067 Å exciting line very strong autoionization structure is observed. This autoionization structure has been attributed to the $n = 4$ member of the Rydberg series converging to 12.86 eV, and as stated earlier the molecular geometry in this Rydberg series is expected to be more bent than the molecular ground state, and for this reason it is unlikely that the autoionizing level could populate the $v' = 0$ level of the ion. The most damaging evidence against the value of 8.8 eV for the ionization potential of NO_2 is the work reported by Fehsenfeld, Ferguson and Mosesman [37]. This experiment involved the charge-transfer reaction between NO_2^+ and NO. A buffer gas was employed to make certain the NO_2^+ was not in an excited state when it reacted with the NO. The NO_2^+ initially was produced by charge transfer from Ar^+. It was observed that

the charge transfer was exothermic and thus it must be concluded that the minimum value for the ionization potential of NO_2 is greater than 9.25 ± 0.02 eV, the ionization potential of NO.

Several other experimental attempts were made to obtain a consistent value for the ionization potential of NO_2 *via* different approaches. One of these was from the fragmentation of CH_3NO_2. Kandell [17] reported an electron impact value for the appearance potential of NO_2^+ from CH_3NO_2 of 9.91 eV, and it looked like a promising molecule to study. Investigation of the fragmentation showed that the first process was not dissociation into CH_3 and NO_2^+ as hoped, but that these products were formed by the third or possibly fourth fragmentation process. With this in mind, the value of 10.0 eV for the ionization potential of NO_2^+ obtained from the present CH_3NO_2 photoionization experiment is within the range of interest, but still too high to be confirmatory.

Another experiment was performed in which the endoergic charge-transfer between NO^+ and NO_2 was attempted. The rationale for the experiment was based on the observation by Fehsenfeld, *et al.* [37] of the exothermic charge-transfer and the hope that the reverse charge transfer could be observed. The experiment proved futile as there was no significant amount of NO_2^+ produced by the reaction. Therefore, although the threshold for the reverse reaction is low

the cross section is apparently too small to be measured with our present arrangement.

One further experiment that was performed was the photodissociation of HNO_3. Good photoionization efficiency curves were obtained for this process, and it appears that fragmentation to the OH radical and NO_2^+ is the first process. Using readily available thermodynamic data [38] for the heats of formation of the fragments of HNO_3, which are listed in Table III, the heat of reaction for the process:

$$HNO_3 \longrightarrow NO_2 + HO \qquad (4)$$

can be calculated. From equation (5),

$$\Delta H_{RXN} = \Delta H^0_{f_{298}}(NO_2) + \Delta H^0_{f_{298}}(HO) - \Delta H^0_{f_{298}}(HNO_3) \qquad (5)$$

and using the values from Table III, the heat of reaction is calculated to be 12.087 eV. Using this value, the appearance potential, and equation (6)

$$I.P.(NO_2) = A.P.(NO_2^+) - \Delta H_{RXN} \qquad (6)$$

the value for the ionization potential of NO_2 is calculated to be 9.94 eV. Again, this value is higher than the photoionization result. A possible explanation for this could be the existence of a potential barrier to the fragmentation, in which case more energy is needed to dissociate the molecule, and thus the fragments leave with excess kinetic or internal energy. Another possibility exists which requires

Table III. Heats of formation for HNO_3, $C_2H_5ONO_2$ and their fragments.

Fragment	$\Delta H^0_{f_{298}}$ (Kcal/mole)	$\Delta H^0_{f_{298}}$ (eV)	Ref
HNO_3	-32.28	-1.40	38
$C_2H_5ONO_2$	-36.82	-1.60	40
HO	9.31	0.404	38
C_2H_5O	- 8.5	-0.369	40
NO_2	7.93	0.344	38

further investigation; it is possible that the heat of formation of one of the fragments or the parent itself is in error. It is highly unlikely that the heats of formation of NO_2 and OH are poorly established, thus indicating that the heat of formation of HNO_3 is incorrect.

Evidence which supports the observed direct ionization potential of NO_2 from this study is obtained from the fragmentation pattern of $C_2H_5ONO_2$ reported by Victor Fong [39]. From the reaction

$$h\nu + C_2H_5ONO_2 \longrightarrow C_2H_5O + NO_2^+ \qquad (7)$$

Fong reported the appearance potential for NO_2^+ to be 11.26 ± 0.01 eV. Again as in the case of HNO_3, using readily available thermodynamic data [38,40] which are presented in Table III the heat of reaction, ΔH_{RXN}, to form the neutral products can be calculated using equation (8):

$$\Delta H_{RXN} = \Delta H^0_{f_{298}}(C_2H_5O) + \Delta H^0_{f_{298}}(NO_2) - \Delta H^0_{f_{298}}(C_2H_5ONO_2). \qquad (8)$$

The ΔH_{RXN} obtained is 1.56 eV. Employing the formula given in equation (6), the ionization potential of NO_2 is found to be 9.7 ± 0.1 eV. This process is not the first fragmentation and as a result the value calculated is probably high; the true ionization potential should be somewhat lower.

Thus, in conclusion it appears that the ionization potential of NO_2 is greater than 9.25 ± 0.02 eV and less

than or equal to 9.62 ± 0.01 eV. There are indications that the value is not very far below the upper limit.

The Dissociation of NO_2

The dissociative ionization of NO_2 into NO^+ and an O atom in a mass spectrometer has been reported by Dibeler, et al. [23], Weissler, et al. [25], Kiser and Hisatsune [19] and Collin and Lossing [16]. As with the ionization potential of NO_2, there is disagreement in the reported appearance potentials of NO^+. However, as may be seen in Table IV, there is a smaller range in the reported values.

The appearance potential of NO^+ from NO_2 can be calculated for the reaction written in equation (9):

$$NO_2(^2A_1) + h\nu \longrightarrow NO^+(^1\Sigma^+) + O(^3P) + e^- \qquad (9)$$

by using standard thermodynamic values given in Table V, the ionization potential of 9.25 eV for NO [41] and equation (10),

$$A.P.(NO^+) = I.P.(NO) + \Delta H^0_{f_0}(NO) + \Delta H^0_{f_0}(O) - \Delta H^0_{f_0}(NO_2). \qquad (10)$$

From the calculation the appearance potential of NO^+ is found to be 12.37 eV, based on the 0^0K values. Dibeler and co-workers [23], as well as Kiser and Hisatsune [19], seem to have found the threshold, within the quoted experimental errors of the techniques employed, where it is predicted to be.

Table IV. Reported threshold values for formation of NO^+ from NO_2.

Technique	Threshold (eV)	Reference
Electron Impact	10.1 ± 0.2	16
Electron Impact	12.48 ± 0.43	19
Photoionization	12.34	23
Photoionization	11.3 ± 0.04	25

Table V. Heats of formation of NO_2 and its dissociation products.[a]

Fragment	$\Delta H^0_{f_0}$ (Kcal/mole)	$\Delta H^0_{f_0}$ (eV)	$\Delta H^0_{f_{298}}$ (Kcal/mole)	$\Delta H^0_{f_{298}}$ (eV)
NO_2 ($^2A_1$)	8.59	0.3725	7.91	0.3430
NO ($^1\Sigma^+$)	21.46	0.9306	21.58	0.9358
O ($^3P_2$)	58.989	2.5581	59.559	2.5828

[a]From reference 42.

As stated in the portion of the experimental section concerned with the fragmentation of NO_2 (Chapter II), NO impurity in the sample was the single most significant problem in these experiments. Even with the provisions outlined in Chapter II to remove this NO impurity, approximately 5% NO impurity remained. The background ion contribution to the efficiency curve from the impurity was subtracted from the raw data by the computer.

Figure 7 shows the photoionization efficiency curve for the NO^+ fragment from NO_2 in the threshold region (1100 - 920 Å). There are two significant aspects to this curve; the first is the possible existence of a very small step 12.37 eV, the thermodynamic threshold, and the second a much stronger series of steps starting at approximately 12.90 eV. This result is in very good agreement with that reported by Dibeler and co-workers [23]. They reported a small peak at 12.34 eV, but not a continuous dissociation, and also observed the strong rise at 13.01 eV. Examination of the photoionization efficiency curve of NO^+ from NO in this region shows the existence of a very strong autoionization peak at 12.34 eV, and it is probable that what Dibeler and others believe to be NO^+ from NO_2 is in fact NO^+ from NO impurity. As can be seen in Figure 7 the step observed at 12.37 eV is very small and it may well be the result of NO impurity not sufficiently corrected for in the data. Although this step could be due to dissociation of the NO_2 molecule, there is no conclusive evidence to make a decision

Figure 7. Photoionization efficiency curve for NO^+ from NO_2 in the threshold region (1000- 920 Å).

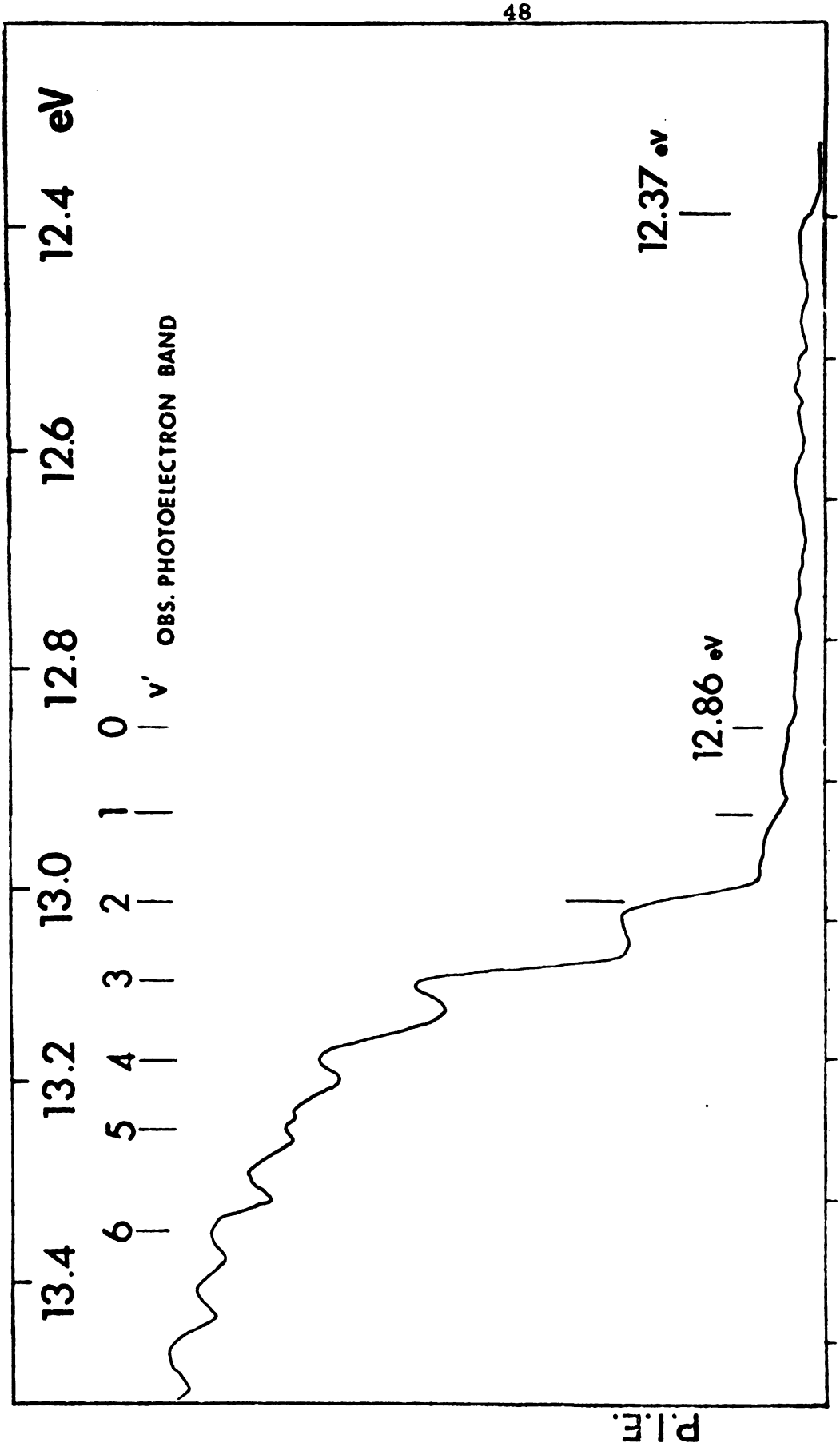
p.i.m.
13.4
13.2
13.0
12.8
12.6
12.4 eV
6
5
4
3
2
1
0
v'
OBS. PHOTOELECTRON BAND
12.37 eV
12.86 eV
920
940
960
980
1000
WAVELENGTH(Å)

Figure 7.

on this point. A possible explanation for this step will be discussed in more detail subsequently. The interesting region of this efficiency curve is from 12.96 to 13.33 eV. The sudden rise in this region can be correlated with an excited ionic state observed by Brundle, et al. [12] and Edquist, et al. [22] in their photoelectron spectra of NO_2, which is located at 12.86 eV and has a vibrational progression associated with it. The vibrational structure observed in this photoelectron band is shown in Figure 7 and has been assigned as a progression in ν_2, the bending mode of NO_2^{+*}. It can be seen in Figure 7 that the $v_2' = 0$ and $v_2' = 1$ vibrational levels show only slight evidence of dissociation while $v_2' \geq 2$ are strongly dissociated. It is clear that this dissociation can occur only via some form of predissociation mechanism.

In order to discuss this predissociation there are some important points which should be made. These are represented schematically in Figure 8. The first is that the ionic ground state of NO_2^+ is a singlet state. Utilizing the Wigner-Witmer correlation rules [32] and using the isoelectronic molecule CO_2 as an example, this lowest singlet state does not correlate with ground state dissociation products because of the violation of the spin conservation rule. However, the first excited ionic state at 12.86 eV, the predissociating state, is a triplet and can correlate with the ground state dissociation products. A second aspect of this dissociation is that the ground state dissociation limit

Figure 8. Potential energy curves representing fragmentation of NO_2.

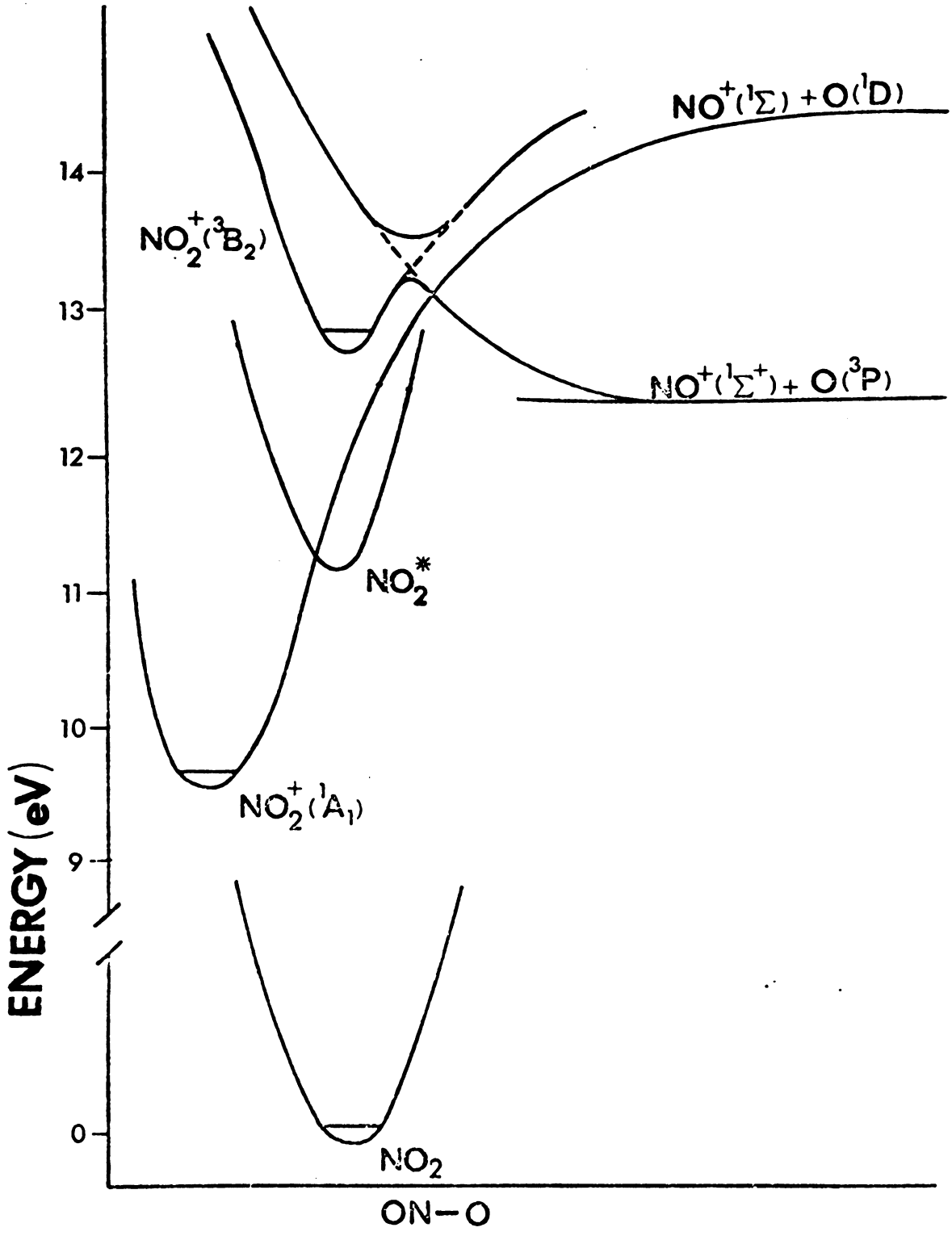
$NO^+(^1\Sigma) + O(^1D)$
$NO^+(^1\Sigma^+) + O(^3P)$
$NO_2^+(^3B_2)$
NO_2^*
$NO_2^+(^1A_1)$
NO_2
14
13
12
11
10
9
0
ENERGY (eV)
ON—O

Figure 8.

(12.37 eV) is lower than the zero point energy of the potential curve for the first excited ionic state at 12.86 eV. The next dissociation limit corresponds to the production of excited oxygen atoms and will be located 1.967 eV above the ground state dissociation limit [43]. In order for the state at 12.86 eV to be dissociated it must go to ground state products at 12.37 eV and thus there must be some form of potential barrier to this process. Again, if one uses the isoelectronic case of CO_2 as a guide, it is expected that the ground state dissociation products can be correlated with a repulsive curve (reference 30, page 431). If this state in NO_2^+ is not linear as it is in CO_2, the repulsive curve originating from it will be split due to the symmetry change giving two repulsive curves. For the dissociation to occur it must go through the antisymmetric stretch. Since there are at least six bound vibrational levels in the bending mode, there must be at least zero point energy in each of the other normal modes.

The potential barrier which must exist to some measure is probably due to the interaction of one of the repulsive surfaces correlating with ground state products with the surface of the excited ionic state at 12.86 eV. If a repulsive state and the excited ionic state are of the same symmetry species, as indeed must be the case for one of the repulsive surfaces arising from ground state products, the interaction of the two electronic states will be so strong as to result in an "avoided crossing". This "avoided

crossing" of course is a result of the non-crossing rule [30], and is represented schematically in Figure 8. The dissociation coordinate represented in the figure is the ON-O bond length. The ground state molecule has a bond length of 1.193 Å [30]. Because the first ionic state of NO_2^+ is isoelectronic with ground state CO_2 it will probably have a comparable bond length, which for CO_2 is 1.16 Å (or perhaps somewhat shorter due to the increased nuclear charge). The first excited ionic state corresponds to the promotion of a π_g electron in the CO_2 molecule to the π_u orbital. This will result in the molecule becoming more bent, but also since the π_u orbital is a formally anti-bonding orbital it will weaken the molecule and the bond strength. Because of this it is probable that the equilibrium bond length of the first excited ionic state is no shorter than in the ground state of the neutral molecule. In Figure 8 only one vibration in ν_3, the antisymmetric stretch, is shown for the $^3B_2$ state of NO_2^+; however, this is merely for purposes of the drawing, since there is no way of telling just how many bound vibrations there are in this degree of freedom.

Looking at the ionization efficiency curve in Figure 7 it is evident that the $v_2' = 0$ and 1 vibrational levels dissociate very little, whereas significant amounts of NO^+ are formed from the higher vibrational states. It thus appears that the effectiveness of the predissociation in some measure depends upon the ability of the bending vibration

to couple with the antisymmetric stretch. If this is the case, the lifetime of the excited ion will be a function of the vibrational level from which the dissociation initiates.

If a comparison is made of peak intensities for each vibrational level observed in the fragmentation spectrum to the peak intensities of these same vibrational levels observed in the photoelectron band, it indeed becomes clear that the probability for dissociation varies as a function of the bending coordinate of the $^3B_2$ ion. This is shown in Table VI as the ratio of NO^+ observed to that of the NO_2^+ from which it originates. This ratio reaches an approximate plateau at $v_2' = 3$ and above implying that all of the NO_2^+ formed in these vibrational states dissociates within the time it is in the ion source, or that all these vibrational levels have the same half-life for dissociation. This point can be checked experimentally by searching for the production of NO^+ by the unimolecular dissociation of metastable NO_2^+ in the mass spectrometer. If an ion decomposes after it has been accelerated from the source chamber, but before it enters the magnetic field, it appears generally at a non-integral mass position given by the formula $m_{meta} = (m_f)^2/m_p$, and it is said to be metastable. (m_f and m_p are the masses of the fragment and parent ions respectively.) Newton and Sciamanna have reported the observation by electron impact [44,45] of a metastable dissociation of NO_2^+ yielding NO^+ fragments. They observed two separate contributions to the metastable peaks, one of low kinetic energy

release and one of high kinetic energy release. It therefore appeared that a search for NO^+ from metastable NO_2^+ produced by photoionization might prove fruitful.

Table VI. Ratio of NO^+ peak height from fragmentation to NO_2^+ peak height from photoelectron spectrum.[a]

V'	NO^+/NO_2^+
0	0.33 ± 0.3
1	0.24 ± 0.2
2	1.29 ± 0.1
3	2.38 ± 0.1
4	2.15 ± 0.2
5	1.93 ± 0.3

[a]From reference 22.

Shown in Figure 9 is the photoionization efficiency curve for the metastable production of NO^+ from NO_2^+; also shown are the positions of the vibrational levels observed in the 12.86 eV photoelectron band. As can be seen, the $v_2' = 0$ level shows only very slight evidence of dissociating in the time it takes the NO_2^+ parent ion to move from the ion source through the field-free region. The $v_2' = 1$ level shows a substantial amount of metastable production, as does $v_2' = 2$. For the higher vibrations, $v_2' = 3$ and greater, there does not appear to be any contribution whatever to the

Figure 9. Photoionization efficiency curve for the metastable production of NO^+ from NO_2.

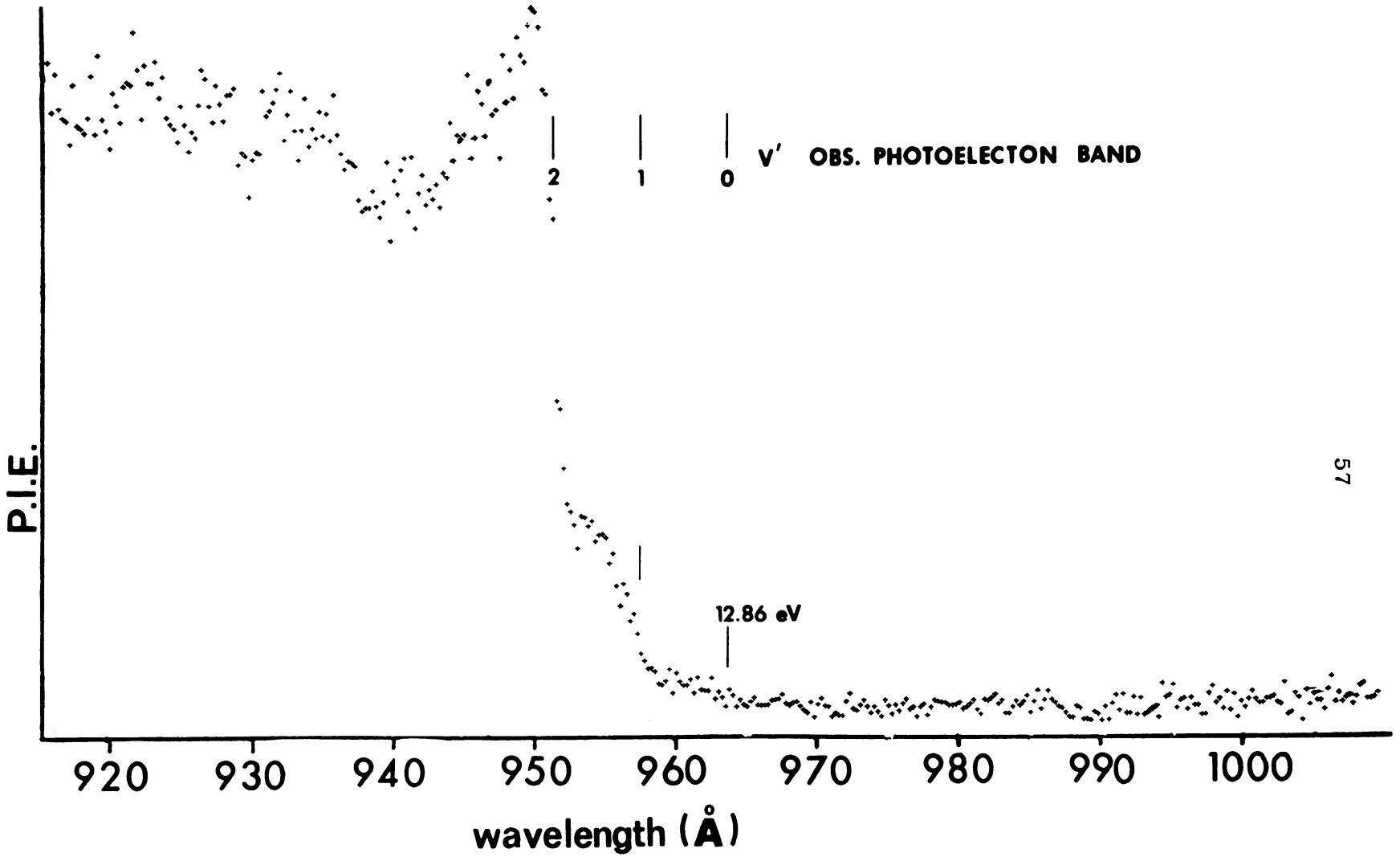
V' OBS. PHOTOELECTON BAND
2
1
0
12.86 eV
P.I.E.
920
930
940
950
960
970
980
990
1000
wavelength (Å)

Figure 9.

metastable curve, which shows that all the parent (or most of it) dissociates in the time it takes to reach the field-free region. An examination of the behavior of the mass peak as a function of the ion accelerating voltage was made to determine the kinetic energy release to the fragments and thus identify which of the two metastables reported by Newton and Sciamanna was being observed. Shown in Figure 10 is a voltage scan of the metastable peak at m/e = 19.55. The exciting wavelength for the measurement was 950 Å (13.04 eV). To calculate the kinetic energy release to the fragments, equation (11) taken from the paper of Newton and Sciamanna [44], was employed.

$$d = \frac{4m_1^2}{m_0} \left(\frac{m_2}{m_1} \frac{T}{eV_A}\right)^{1/2} , \qquad (11)$$

m_0 is the mass of the parent, m_1 the mass of the observed fragment, m_2 the mass of the other fragment, T is the kinetic energy release, V_A is the ion accelerating voltage and d is the half-width of the voltage scan at 70% full height in mass units. Making this calculation yields a kinetic energy release of 0.59 eV to the fragments, which is in excellent agreement with the value of 0.51 eV reported by Newton and Sciamanna for their low kinetic energy component [44]. The relatively steep sides of the curve in Figure 10 indicate that there is relatively little spread in the kinetic energy release. Further, by producing the parent NO_2^{+*} with a photon beam of 13.04 eV it is

Figure 10. Voltage scan of metastable peak at m/e = 19.57.

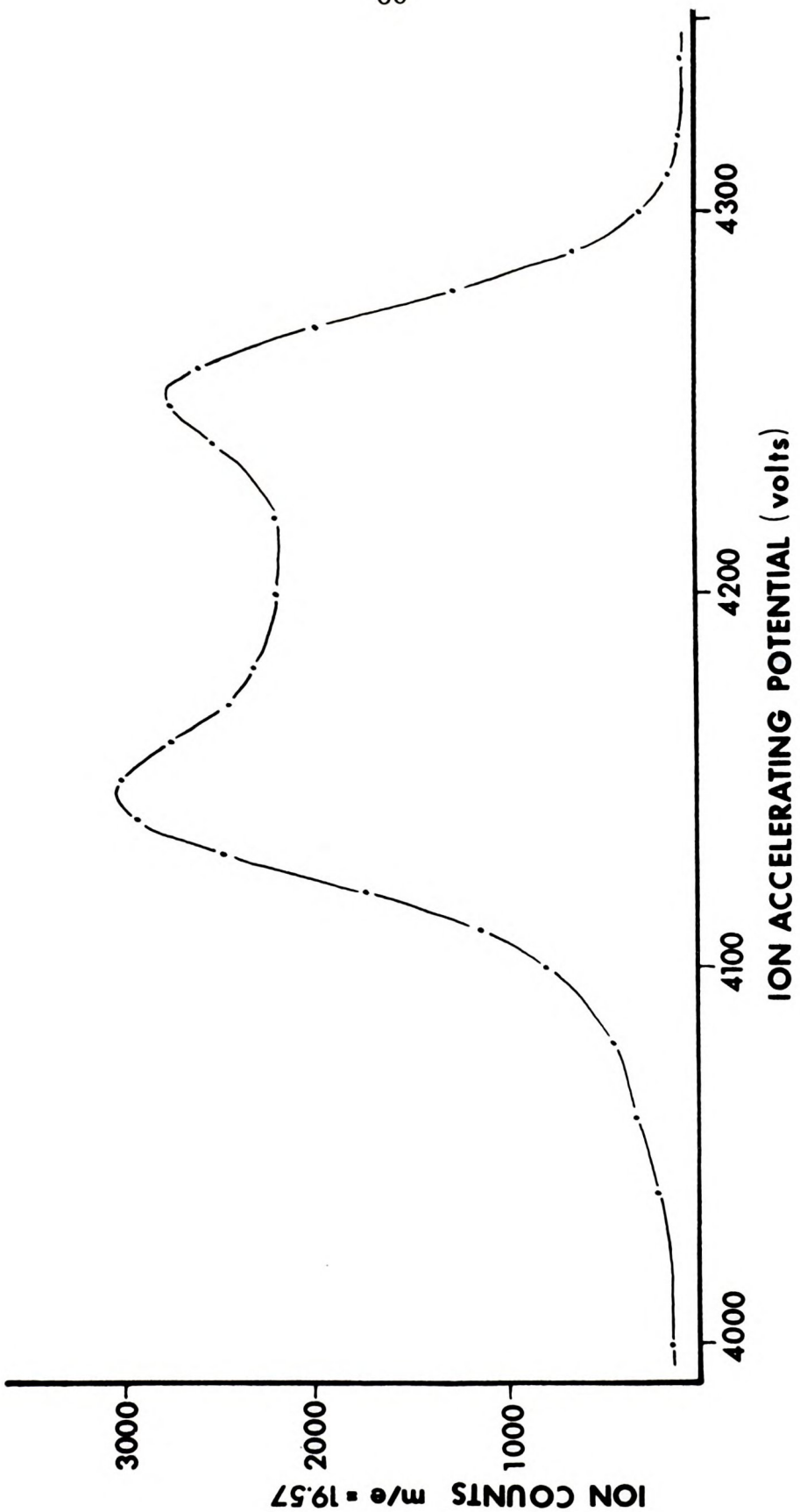
ION COUNTS m/e = 19.57
3000
2000
1000
4000
4100
4200
4300
ION ACCELERATING POTENTIAL (volts)

Figure 10.

selectively made in vibrational levels of $v_2' \leq 2$. With the thermodynamic threshold at 12.37 eV the parent ion NO_2^+ has excess energy of 0.67 eV when in $v_2' = 2$, but on the average about 0.59 eV of this exess energy is given up to the fragments as kinetic energy. The lowest vibrational spacing in NO^+ is 0.28 eV so it is clear that very little if any NO^+ is formed with excess vibrational energy.

From information about the production of NO^+ fragments within the ion source and the metastable production of NO^+ originating from the same electronic state of NO_2^{+*}, it is possible to calculate the half-lives of the various vibrational levels for this dissociation. To make this calculation one needs to know the residence time of the NO_2^+ parent ions in each region of the mass spectrometer. These times can be calculated directly from the knowledge of the dimensions of each region, the strengths of any electric fields present, and simple classic mechanics.

First, it is easiest to calculate the half-life of the $v_2' = 3$ level. Because no detectable amount of NO^+ originating from the vibration is seen in the metastable curve one may make the assumption that at least 90% of the NO_2^+ formed in $v_2' = 3$ dissociates in a time shorter than 16 μsec, the time it takes the ions to reach the field-free region in this experiment. (Repeller voltage = 0.8 V.) Using this conservative estimate and assuming the decay is first order, the half-life is calculated to be ≤ 4.8 μsec. To calculate the half-life of the $v_2' = 2$ level the information in Table VI

must be utilized. As can be seen, the ratio of the peak heights is diminished 55% from the value expected if the half-lives of the $v_2' = 3$ and $v_2' = 2$ states were the same and all other effects were equal. By calculating how much NO_2^+ in the $v_2' = 3$ level had dissociated in the time the ions are in the source chamber, and assuming 55% less dissociation for $v_2' = 2$, a rough estimate of how much NO_2^+ in the $v_2' = 2$ level has dissociated in the same amount of time can be made. Again assuming first-order decay, the half-life of $v_2' = 2$ is approximately 11 μsec.

The calculation of the half-life of $v' = 1$ and $v' = 0$ is somewhat more involved. The information needed to do this calculation must come from the metastable photoionization curve. All the intensity in this curve comes from the dissociation of NO_2^{+*} while the electronically excited ion is in the field-free region. The intensity (area) of each peak can be expressed mathematically assuming first order decay kinetics. t_a is the time it takes the NO_2^{+*} to reach the field-free region from the source and t_b is the time it takes to pass from the source through the field-free region. The concentration of NO_2^{+*} that decays while in the field-free region can be calculated. The amount of NO_2^{+*} in some particular vibration $v_2' = X$ present at time t_a is A_{Xa} and the amount present after passing through the field-free region is A_{Xb}. The difference between these two numbers is the amount of NO_2^{+*} which has decomposed, and therefore

the amount of NO^+ that should be observed in the metastable photoionization efficiency curve. The equations necessary to perform this calculation are:

$$A_{Xa} = A_{Xo} e^{-k_x t_a} , \qquad (12a)$$

$$A_{Xb} = A_{Xo} e^{-k_x t_b} , \text{ and} \qquad (12b)$$

$$A_{Xa} - A_{Xb} = A_{Xo}(e^{-k_x t_a} - e^{-k_x t_b}), \qquad (12c)$$

where A_{Xo} is the concentration of NO_2^{+*} in the vibrational state $v_2' = X$ at $t = 0$ and k_x is the rate constant for dissociation. To continue the calculation, measurements of the ratio of the observed peak heights in the metastable curve relative to $v_2' = 2$ can be made. This ratio is called R_m^* and is given by equation (13):

$$R_m^* = \frac{P.H.(v_2' = 2)}{P.H.(v_2' = X)} , \quad X = 0,1. \qquad (13)$$

R_m^* may be expressed mathematically using equation (12c):

$$R_m^* = \frac{A_{2a} - A_{2b}}{A_{Xa} - A_{Xb}} = \frac{A_{2o}(e^{-k_2 t_a} - e^{-k_2 t_b})}{A_{Xo}(e^{-k_x t_a} - e^{-k_x t_b})} , \quad X = 0,1. \qquad (14)$$

In this equation k_2 is known from previous arguments, and therefore equation (14) reduces to:

$$R_m^* = \frac{A_{2o}\ 0.134}{A_{Xo}(e^{-k_x t_a} - e^{-k_x t_b})} \quad . \qquad (15)$$

In equation (15) there are three unknowns: A_{2o}, A_{Xo}, and k_x. The ratio A_{2o}/A_{Xo} may be found utilizing the photoelctron results of Brundle [12] by taking the reported peak heights. It should be noted that the effects of autoionization are absent in the photoelectron spectra, and that the photoelectron cross-section is energy dependent. Thus, the ratio of the photoelectron peak heights is not an exact measure of the relative NO_2^{+*} concentrations in the photoionization experiment. This ratio of the observed Franck-Condon factors is called $R_{F.C.}$ and is given by equation (13) except R_m^* is replaced by $R_{F.C.}$. Substituting this value into equation (15) and rearranging yields:

$$e^{-k_x t_a} - e^{-k_x t_b} = \frac{R_{F.C.}\ 0.134}{R_m^*} \quad . \qquad (16)$$

There is only one unknown in this equation, k_x, which may be determined graphically. The measured values of $R_{F.C.}$ and R_m^* for $v_2' = 0$ and 1 are given in Table VII. These same calculation can be repeated starting with the assumption that 100% of the NO_2^{+*} formed in $v_2' = 3$ dissociates in a time shorter than 10.15 μsec, the time it takes the ions to reach the field-free region. The results of both calculations are presented in Table VIII; they indicate a striking dependence of the half-life of the NO_2^{+*} ion on the number of bending vibrational quanta excited.

Table VII. Experimental data used to solve equation (16).

v_2'	R_m*	$R_{F.C.}$[a]
0	18.7	3.2
1	3.1	1.3

[a]See reference 12.

Table VIII. Summary of results from the calculation of the lifetimes for dissociation of the vibrational levels of the $^3B_2$ state of NO_2^+.

v_2'	Upper Limit $\tau_{1/2}$ (μ sec)	Lower Limit $\tau_{1/2}$ (μsec)
0	154.6	147.4
1	57.8	53.3
2	16.2	13.9
≥ 3	≤ 4.8	≤ 2.4

The small rise in the photoionization efficiency curve (Figure 7) at 12.37 eV requires some explanation. It is probably due to NO impurity; however, it might be accounted for in two other ways. First there may be a Rydberg level in the vicinity which simultaneously autoionizes and predissociates into one of the repulsive curves originating from the ground state dissociation products. One problem

with this interpretation is that after the onset there is almost continuous fragmentation. If this originates from a Rydberg level it should be discrete unless there is an extremely dense population of predissociating Rydberg levels. The second possibility is that an optical transition is made to the ground ionic state, and in the time the NO_2^+ ion remains in the ionization chamber it makes a forbidden transition into the dissociation continuum. This would require a spin change, but this may happen since the sample resides in the source $\sim$ 11 μsec, which may be long enough for the multiplicity change. One argument against this process is that the Franck-Condon factors for the optical transition to the ionic curve are most probably so small that the process would not be observed.

In Figure 11 the NO^+ photoionization efficiency curve is compared with the NO_2^+ parent curve. It may be noted that the two curves show identical structure, which is due to the fact that the Rydberg levels which appear as autoionization structure in the parent curve may also competitively predissociate, therefore appearing in the fragment curve as well. This is illustrated by equation (17):

$$NO_2 + h\nu \longrightarrow NO_2^* \begin{cases} \nearrow NO_2^+ + e^- \\ \searrow NO^+ + O + e^- \end{cases} . \qquad (17)$$

In conclusion, if the NO^+ observed at the thermochemical limit is not an artifact, it is probably due to

Figure 11. Comparison of NO^+ and NO_2^+ photoionization efficiency curves.

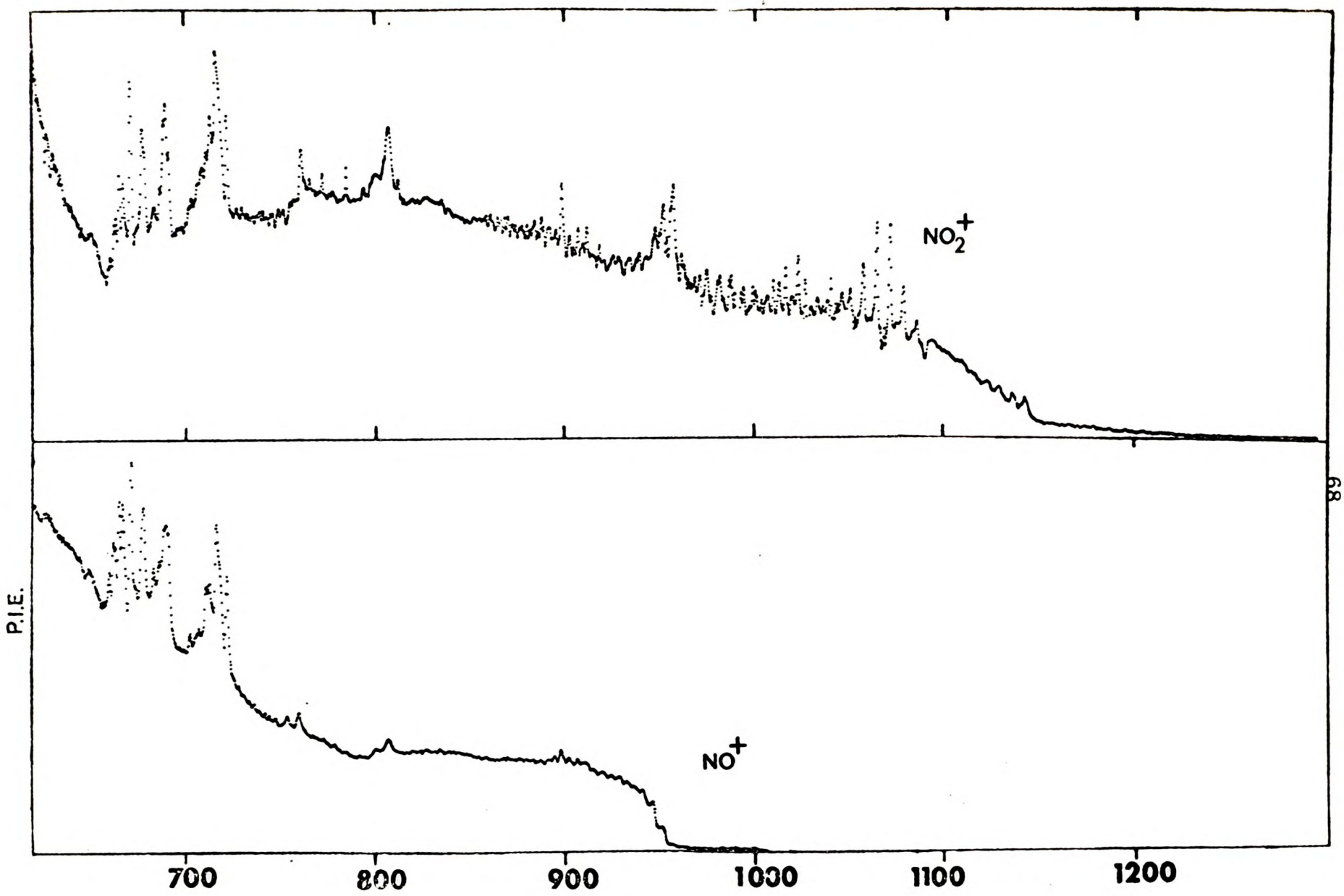

Figure 11.

some form of predissociation. There is, however, no way to say with certainty that this onset is real. The striking structure observed at and above 12.86 eV has been explained as due to predissociation of the first excited ionic state ($^3B_2$) and the lifetimes of the various bending vibrational levels of this state have been calculated. However, the details of the dissociation mechanism(s) involved are still uncertain.

RYDBERG ANALYSIS OF NO_2

Introduction

A series of lines corresponding to transitions from the ground state of a molecule to more and more highly excited states of a molecule form a Rydberg series, in analogy with atoms. In 1885 Balmer identified a series of lines in the spectrum of atomic hydrogen due to promotion of the 1s electron to higher and higher atomic orbitals. He found an equation to describe this series which was generalized by Rydberg and this series is now called a Rydberg series. In the more highly excited states of a molecule the higher the orbital energy the more the orbital looks like an atomic orbital. Thus transitions to these orbitals behave like atomic spectra and form Rydberg series. Rydberg series in molecules may be expressed mathematically by the Rydberg formula:

$$\nu_n = \nu - \frac{R}{(n - \delta)^2} \quad , \qquad (18)$$

where ν_n is the observed frequency of the Rydberg transition, ν is the frequency of the convergence limit (this corresponds to complete removal of the electron), R is the Rydberg constant, n is the quantum number of the Rydberg level, and δ is the quantum defect which is a

correction term which accounts for effects such as Rydberg orbital penetration into the molecular core. In molecules, Rydberg orbitals have designations analogous to atomic orbitals np, ns, etc. which come from the united atom approximation followed by the symmetry of molecular orbital formed, a_1, σ, b_2, etc. (For a more detailed discussion of Rydberg series see references 30,32,46.)

The Rydberg analysis of NO_2 has proven to be a very difficult problem. Tanaka and Jursa [15], Nakayoma, Kitamura and Watanabe [11], and Price and Simpson [14] have investigated the vacuum ultraviolet absorption spectrum of this molecule and assigned several Rydberg transitions. All had similar problems in their analyses. The first was the diffusness of the spectra, due in part to the transitions themselves, due to the continuous background absorption, and due to the effect of the sample gas on the photographic plate. Second, and more significant, these investigators did not know in advance the values of the ionization potentials of NO_2. Brundle [12] and Edquist, et al. [22] have since established the positions and accompanying vibrational structure of the ionization potentials of NO_2 up to 21 eV by photoelectron spectroscopy. The vibrational structure near the ionization limits is extremely useful when trying to assign Rydberg transitions, since each member of a series should exhibit the same type of structure as the limit to which it converges. Utilizing the information from their photoelectron spectra, the previously observed absorption

spectra, and the photoionization efficiency curve reported by Dibeler, et al. [23], Edquist and co-workers suggested assignments for many of the Rydberg transitions in NO_2. The photoionization efficiency curve of NO_2^+ obtained in this investigation exhibits substantial autoionization structure. Using the assignments of Edquist, et al. [22] as a guideline, most of this structure can be identified.

Assignment of the Autoionization Structure

The first excited ionic state at 12.86 eV corresponds to the removal of an electron from the $3b_2$ orbital. Tanaka and Jursa [15] and Nakayama, et al. [11] have observed a series converging to 12.86 eV. Edquist, et al. [22] have assigned this as the $3b_2 \longrightarrow ns\sigma$ transition, based on the quantum defect having a value of approximately 1.00. While only two members of this Rydberg series have been seen previously, four members of the series are observed in the photoionization spectrum. Table IX lists the positions of each member of the series and the positions and quantum defects of the vibrational levels associated with each member. This vibrational structure has been assigned as a progression in ν_2, the bending vibration. The $v_2' = 0$ vibrational level is not observed for the $n = 3$ and $n = 4$ members of the Rydberg series in autoionization. A possible reason for this behavior is that the $v_2' = 0$ vibrational levels of these states do not overlap the ionization continuum sufficiently to autoionize (see discussion on the ionization

Table IX. A Rydberg series converging to 12.86 eV: $3b_2 \longrightarrow ns\sigma$

n	V'	Observed (Å)	Tanaka and Jursa[a]	δ
3	0		1293.3	
	1	1282.30	1283.2	0.96
	2	1272.80	1273.2	0.96
	3	1262.50	1263.4	0.96
	4	1253.55	1253.8	0.97
	5	1243.43		0.97
	6	1234.30		0.97
4	0		1092.8	
	1	1.085.46	1085.4	1.01
	2	1077.66	1078.1	1.01
	3	1070.46	1070.9	1.01
	4	1063.46	1063.8	1.01
	5	1056.26	1057.0	1.01
5	0	1033.15		1.02
	1	1026.40		1.02
	2	1019.40		1.02
6	0	1006.15		0.99
	1	999.90		0.99

[a]From Reference [15].

potential of NO_2). When going to higher members of the series this problem is no longer a factor and the $v_2' = 0$ level can autoionize. There is much more structure in the region of the convergence limit, probably due to the higher members of the Rydberg series piling up. Because of this effect many lines are closely spaced and probably perturb one another making it impossible to assign all these lines.

Edquist, et al. [22] have assigned the strong band at 1142.6 Å in the photoionization curve as due to a $1a_2 \rightarrow$ npσ Rydberg series converging to 13.60 eV. This band is strong and exhibits little evidence of vibrational structure implying, based on the photoelectron band shapes of Edquist, et al. [22], that this band may be converging to either 14.07 eV or 18.86 eV, if it is due to a Rydberg transition. If this band is a member of a Rydberg series converging to 14.07 eV it would have a quantum defect of 0.96, indicating a nsσ type transition. It is probable that the ionic state at 14.07 eV is bent; since this state results from the promotion of a $1a_2$ electron the transition is forbidden because of the dipole selection rule. A second argument against this interpretation is that no other member of the series can be identified. If, on the other hand this band is a member of a Rydberg series converging to 18.86 eV it will have a quantum defect of 0.70, in line with a npσ type transition. The state at 18.86 eV is also probably bent, however, the npσ transition is dipole allowed. Utilizing this quantum defect two more members of this series

may be assigned. Table X presents a summary of the positions of each member of the series and the quantum defects of each member. Four other series have previously been reported converging to 18.86 eV by Tanaks and Jursa [15], but this possible series was not so designated. The band at 1142.6 Å was assigned as the $v_2' = 0$ member of a progression Tanaka and Jursa [15] had placed in a Rydberg series converging in the vicinity of 12.0 eV. The first and third members of that series have since been assigned as the first two members (n = 3,4) of a Rydberg series converging to 12.86 eV [12]. The remaining part of this progression reported by Tanaka and Jursa [15] has been assigned by Edquist, et al. [22] as the $3b_2 \rightarrow nd\sigma$ transition converging to 12.86 eV. Examination of the photoionization efficiency curve shows the presence of three members of this progression. However, there is no evidence for any higher members of the Rydberg series converging to 12.86 eV reported by Edquist, et al. [22]. The second member (n = 4) of this Rydberg series is expected to appear at approximately the same place the second member of the $ns\sigma$ series converging to 12.86 eV; perhaps it is obscured by the intense lines due to the transition. Thus it remains unclear whether the assignment of this progression as a Rydberg series converging to 12.86 eV by Edquist, et al. [22] is correct and no conclusion may be made on the basis of this data.

Table X. A new Rydberg series converging to 18.86 eV: $2b_2 \rightarrow np\sigma$.

n	V'	Observed (Å)	δ (calc)
2	0	1142.60	0.72
3	0	760.40	0.70
4	0	702.60	0.66

In the vicinity of 1020 Å three bands tend to stand out more prominently than the rest. Most of the structure in this region has been attributed to the piling up of the Rydberg series converging to 12.86 eV (968 Å). However, because of the anomalous intensity of these bands it might be assumed that they are converging to a higher ionization potential. From the photoelectron spectrum of Edquist, et al. [22] it is possible that these bands are converging to 14.07 eV. If this is the case, the series would have a quantum defect of approximately 0.40 in line with a $1a_2 \rightarrow np\pi$ type transition which is optically allowed. An extrapolation to the next member of the series predicts a band at approximately 950 Å where such a band is located. The 950 Å band also exhibits a similar intensity distribution in its vibrational structure as the preceding member of the series. No other member of this series can be found. Therefore the assignment must be considered tentative. Table XI presents the information about this series.

Table XI. A possible Rydberg series converging to 14.07 eV: $1a_2 \rightarrow np\pi$.

n'	ν_1	ν_2	ν_3	Observed (Å)	δ
3	0	0	0	1022.40	0.35
	0	1	0	1015.65	0.36
	1	0	0	1012.40	0.35
	0	2	0	1009.15	0.38
4	0	0	0	954.90	0.47
	0	1	0	950.65	0.51
	1	0	0	946.65	0.47

In the region of 1089 Å there is a very smooth and pronounced dip in the photoionization efficiency curve. This dip is not an artifact produced by the light source and is quite reproducible. There is some evidence of a second dip in this region, but it occurs between two strong autoionization lines. It is possible these dips are a manifestation of the phenomenon described by Fano [33] as a window resonance. If this is a window resonance there might be other such "resonances" in the photoionization efficiency curve which would form a Rydberg series. Several attempts were made to fit this band to a Rydberg series. If 18.86 eV is taken as the convergence limit then the band does seem to fit into some type of Rydberg series. A second

member may be seen in the vicintiy of 758 Å. This band also appears to have a second component with it. A third member of the series is expected to be at 700 Å. A very small dip is present in this region; but its assignment as a member of the series is open to question. Table XII presents the information relative to this sereis, which has an average quantum defect of 0.60 in line with a $nd\sigma$ type transition.

Table XII. A Rydberg series converging to 18.86 eV: $2b_2 \rightarrow nd\sigma$.

n	v'	Observed (Å)	δ (calc)
2	0	1089.65	0.65
	1	1081.15	0.65
3	0	752.60	0.62
	1	746.80	0.60
4	0	698.60	0.50

The majority of the remaining structure in the photoionization efficiency curve may be assigned as Rydberg series converging to 18.86 eV which have been identified by Tanaka and Jursa [15]. Table XIII presents a comparison of series I reported by Tanaka and Jursa [15] with the autoionization structure of this work. All seven members of the

Table XIII. Comparison of experimentally observed Rydberg series with series I reported by Tanaka and Jursa[a]: $2b_2 \rightarrow np\pi \rightarrow 18.86$ eV.

n	v'	Observed (Å)	Tanaka and Jursa[a]	δ
2	0	897.10	897.02	0.36
3	0	721.46	721.20	0.16
4	0	691.06	691.01	0.16
5	0	678.26	678.31	0.16
6	0	671.26	671.59	0.18
7	0	666.86	667.39	0.04
8	0	665.26	664.96	0.14

[a]From reference 15.

series reported by Tanaka and Jursa[15] are found in the present study; however, the n = 6,7, and 8 members have an anomalous intensity behavior. The n = 6 band has an intensity significantly greater than any other member of the series and it seems likely that this particular band is a member of some other series converging to a higher ionization potential. This line is included in Table XIII for comparison, although its validity in the series is not established. The n = 2 member of this series was reported by Edquist, et al. [22] to be due to NO impurity lines in the spectrum of Tanaka and Jursa [15]. Since the line is observed in the photoionization efficiency curve and a mass spectrometer is used as the ion detector, the possibility that this line is due to NO impurity is precluded.

Series II reported by Tanaka and Jursa [15] is not observed in the photoionization efficiency curve at all. They reported this series to be weak in absorption, and if this is coupled with an unfavorable autoionization cross section its absence would be understandable. The remaining two series, III and IV, reported by Tanaka and Jursa [15] have been combined into one by Edquist, et al. [22]. This was prompted by the belief that one member of series IV was again due to NO impurity; however, the line in question (783.86 Å) has been observed in the photoionization efficiency curve and therefore cannot be due to NO^+. Thus the two series have been kept intact. Table IV presents a comparison of Series III of Tanaka and Jursa [15] with the

Table XIV. Comparison of experimentally observed Rydberg series with Series III reported by Tanaka and Jursa[a]: $2b_2 \rightarrow ns\sigma \rightarrow 18.86$ eV.

n	Observed (Å)	Tanaka and Jursa (Å)	δ (calc)
3	810.66		1.05
	805.86	806.06	1.03
4	717.00	717.57	1.06
	715.86	715.67	1.03
5	689.66	689.80	1.07
	688.66	688.56	1.02

[a]From reference 15.

Table XV. Comparison of experimentally observed Rydberg series with Series IV reported by Tanaka and Jursa[a]: $2b_2 \rightarrow nd\delta \rightarrow 18.86$ eV.

n	Observed (Å)	Tanaka and Jursa (Å)	δ (calc)
2	792.86		-0.05
	783.86	784.93	-0.14
3	712.86	712.25	-0.04
	710.46	710.43	-0.10
4	687.66	687.52	-0.04
	686.66	686.01	-0.10

[a]From reference 15.

experimental data. Each member of this series was reported to be a doublet by Tanaka and Jursa [15]; however, they did not see the second component. This component has been observed in this photoionization study and is included in the table. Table XV presents a similar comparison between series IV of Tanaka and Jursa [15] and the experimentally observed lines. Again each member of the series was described as a doublet and the second component of $n = 3$ has been added to the table. There are several other lines in this region (650 Å), but they do not fit well into any of these series. Tanaka and Jursa [15] have suggested that because so many series are converging on this limit the lines may be perturbing each other, making assignment virtually impossible.

The line at 671.26 Å, which as previously stated appears to be too intense to be a member of series I converging to 18.86 eV, may belong to a Rydberg series converging to a higher ionization potential. From the photoelectron spectrum the only remaining possibility is the limit at 21.26 eV. Making this assumption yields a quantum defect of 0.79 for $n = 3$ converging to this limit; however, no other line can be associated with this one. Possibly it is converging to a still higher ionization potential.

Figure 12 presents the photoionization efficiency curve of NO_2 with a summary of the various Rydberg series assignments.

Figure 12. Rydberg series of NO_2.

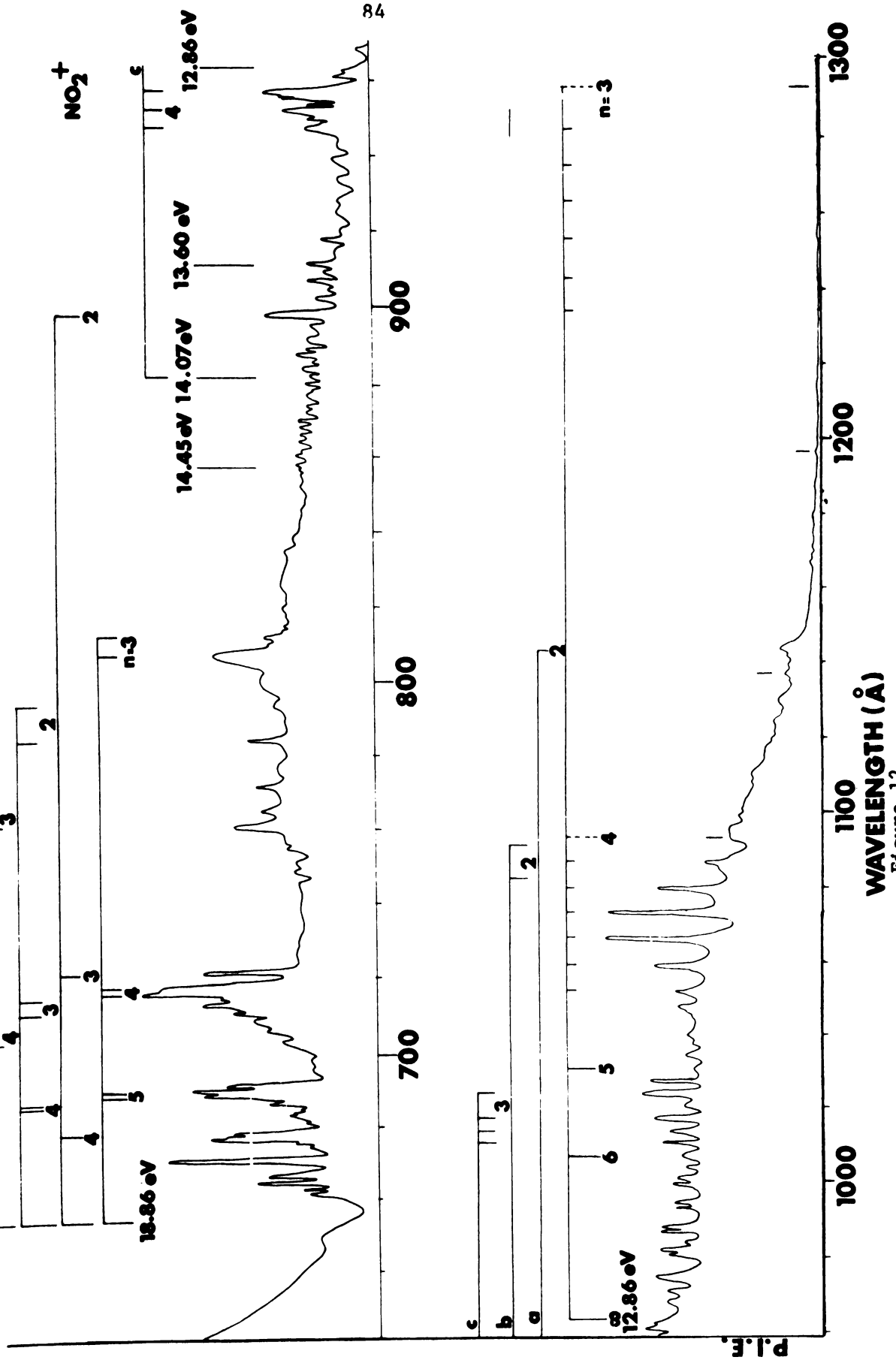
NO_2^+
18.86 eV
14.45 eV
14.07 eV
13.60 eV
12.86 eV
12.86 eV
n=3
n=3
700
800
900
1000
1100
1200
1300
WAVELENGTH (Å)
P.I.E.

Figure 12

THE PHOTOIONIZATION OF NO

Introduction

It has been pointed out by Wigner and others [1-3] that the threshold law for direct ionization by photon impact should be approximately a step function. That is, the cross section for ionization at the threshold should be finite and vary only slowly with energy in the region above this ionization limit until a new limit is encountered. In order to observe this behavior, however, certain other factors must be favorable. In all polyatomic and diatomic molecules there exist Rydberg series converging to the first and each subsequent ionization limit. Those excited neutral states which lie above the first ionization potential of the molecule may autoionize, predissociate or fluoresce. The rate of fluorescence emission is usually much smaller than that of the first two processes and is usually negligible. If these states autoionize they will cause peak-like structure to be superimposed on the step and therefore it may become difficult to distinguish where the next step occurs. In order to observe step-like behavior these excited neutral states must be depopulated by some mechanism which does not yield the charge species of

interest. The mechanism most able to do this is predissociation of the excited neutral states into neutral fragments or charged fragments. The restriction in this case is that the predissociation rate be much faster than the competing autoionization process.

The classic example used to demonstrate step function behavior at threshold has been the NO molecule. Watanabe, Marmo and Inn [47] reported one of the earliest photoionization studies, which revealed three steps in the threshold region of the NO^+ ion corresponding to vibrational levels of the ion. Since that time various other investigators have reported the photoionization cross section curve for this molecule [48-51]. All of these results are in essential agreement that the molecule exhibits step-like behavior over the first four vibrational levels of the ion. One of these investigators [49] used the fact that the cross section was a step function as a standard to calibrate the photon detector. This step-like behavior has been assumed to exist because the neutral excited states are completely predissociated.

As the preliminary step for a charge-transfer experiment a cursory photoionization study of NO was undertaken using 300 micron slits and the hydrogen lamp. Examination of the photoionization efficiency curve in the threshold region revealed some unusual structure on the steps, which obscured the step somewhat. In an attempt to determine if

this structure was real or an artifact of the hydrogen lamp a careful study of NO was undertaken.

The Threshold Region (1350 - 1220 Å)

Shown in Figure 13 is the photoionization efficiency curve of NO in the threshold region, obtained utilizing 100 micron slits. As is evident, there is significant structure superimposed upon the step. Since these data were taken using the smooth Argon continuum as a light source rather than the many-lined psuedo-continuum of the hydrogen lamp, the structure must be considered real. Watanabe [48] and Miescher [52] have investigated the absorption spectrum of NO in this region (1400 - 1300 Å). Miescher [52] used a 10-meter spectrograph for his study and has performed a very detailed analysis of the spectrum. He identified several Rydberg series converging to excited vibrational levels, $v' > 0$, of the ground state $X'\Sigma^+$ of the NO^+ ion. This structure may be correlated with the autoionization structure in the photoionization efficiency curve. Because these Rydberg states are converging to vibrationally excited states of the first ionic state it is evident that this autoionization structure is due to vibrational autoionization. As can be seen in Figure 13 most of these autoionization lines are weak and are fairly well predissociated, but a small probability (of the order of a few percent) of competing autoionization does exist.

Figure 13. Photoionization efficiency curve of NO^+ from NO in the threshold region.

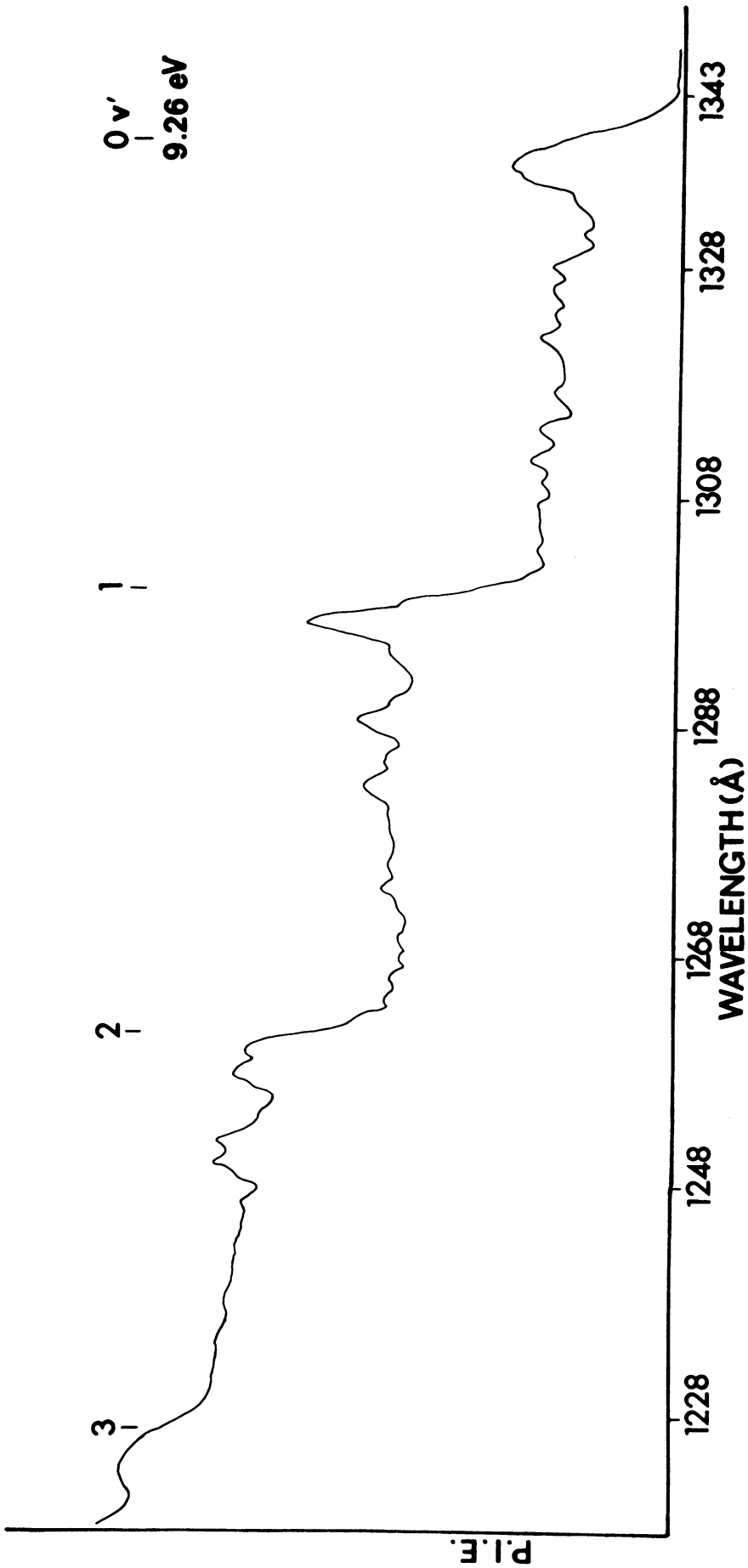
0 v'
9.26 eV
1
2
3
P.I.E.
1228
1248
1268
1288
1308
1328
1343
WAVELENGTH (Å)

Figure 13.

An attempt has been made to assign the structure in the photoionization cross section curve using the assignments of Miescher [52]. Since the instrument used in this experiment does not have the resolution available to Miescher, several possibilities exist for some assignments.

Presented in Table XVI is the assignment of the lines observed on the first vibrational step of the photoionization efficiency curve. A comparison is made between the observed lines and tnose reported by Miescher [52]. In some cases two assignments were possible; in these instances the quantum defect was used to make a decision between the two. Both possibilities are presented in the Table for comparison, with an asterisk used to denote the more likely choice.

The most important aspect of these assignments is the convergence limits of each line. As can be seen from Table XVI, all but one line can be assigned as Rydberg states converging to $v' \geq 2$ of the ground ionic state. Therefore, all of these states converging to $v' \geq 2$ must make a vibrational energy change of at least two quanta in order to autoionize. Berry [35] has proposed a propensity rule for autoionization by vibration in which he states the probability of autoionization should be greatest for a vibrational energy change $\Delta v = 1$, with decreasing probability as Δv increases. The autoionization structure observed on the first step does not disprove or confirm this propensity rule. In this case if these states are to autoionize at all they

Table XVI. Assignment of autoionization structure on the first vibrational step of NO^+ [a].

Observed (Å)	Miescher[b] (Å)	Assignment[c]	δ (calc)	δ^b
1337.17	1340.21(h)	6sσ → v' = 2	+1.19	+1.208
1336.17	1335.92	5dδ → v' = 2	+0.16	+0.078
1334.17	1333.81	5f → v' = 2	+0.12	+0.020
1331.13	---	5sσ → v' = 3	+1.00	+1.201
		4dσ → v' = 3*	+0.00	-0.033
1328.42	---	5d → v' = 2	-0.07	---
		4d → v' = 3*	-0.05	-0.033
1326.42	---	6pπ → v' = 2	+0.84	+0.76
1324.42	---	9pπ → v' = 1*	+0.75	≈+0.76
		6pσ → v' = 2	+0.77	+0.69
1322.42	---	6pσ → v' = 2*	+0.68	+0.69
		5pπ → v' = 3	+0.82	+0.76
1317.67	---	5pπ → v' = 3	+0.74	+0.76
1314.42	1212.80	7sσ → v' = 2	+1.38	+1.217
1311.67	---	5pσ → v' = 3	+0.62	+0.69
1309.92	1310.07(h)	6f → v' = 2	+0.13	+0.029

[a] The vibrational quantum number is that of the limit to which the series converges and also that of the ion core of the Rydberg state. The ion resulting from autoionization will of course have a lower vibrational quantum number.

[b] See reference 52.

[c] When more than one assignment is possible an asterisk is used to indicate the author's choice of the two.

must do so by changing vibrational energy by two quanta. Also since there is only one line converging to $v' = 1$ and it is also very weak it is impossible to estimate if this state has a higher probability of autoionizing than any other state. The intensity of the observed autoionization structure is not only a function of the autoionization rate, but of the rates of the competing processes. Predissociation will have a rate which is dependent (often strongly) upon the vibrational state of the Rydberg level. Thus strong autoionization structure might imply that the predissociation is weak rather than the autoionization is strong. The absence of any other $v' = 1$ lines may be due to a much stronger predissociation of this vibrational level. Examination of Miescher's spectrum [52] shows that he does not observe in absorption any $v' = 1$ levels above the first ionization limit. It is possible these levels are so predissociated they blend into the continuum and thus one would not expect to see any contribution from these in the photoionization experiment.

Table XVII presents the assignments of the observed autoionization structure superimposed on the second vibrational step of the photoionization efficiency curve. There are three strong lines with decreasing intensity and they all have the same quantum defect and appear to belong to the same Rydberg series. In this case these states are converging to the $v' = 2$ vibrational level of the NO ionic ground state. It is interesting to note that these lines

Table XVII. Assignment of autoionization structure on the second vibrational step of NO^+.

Observed (Å)	Assignment	δ (calc)	δ^a
1297.42	$8p\pi \rightarrow v' = 2$	0.77	0.76
1290.42	$5f \rightarrow v' = 3$	0.03	0.029
1288.92	$9p\pi \rightarrow v' = 2$	0.75	0.76
1285.42	?		
1283.17	$10p\pi \rightarrow v' = 2$	0.78	0.76
1274.17	$6d \rightarrow v' = 3$	-0.06	-0.03
1269.92	$7p\sigma \rightarrow v' = 3$	0.68	0.69
1267.67	?		

[a]Average value for observed series from Miescher, reference 52.

Table XVIII. Assignment of autoionization structure on the third vibrational step of NO^+.

Observed (Å)	Assignment	δ (calc)	δ^a
1260.42	$8p\pi \rightarrow v' = 3$	0.77	0.76
1258.42	$8p\sigma \rightarrow v' = 3$	0.62	0.69
1252.67	$9p\pi \rightarrow v' = 3$	0.75	0.76
1250.92	$9p\sigma \rightarrow v' = 3$	0.54	0.69
1247.42	$10p\pi \rightarrow v' = 3$	0.78	0.76

[a]Average value for observed series, from Miescher, reference 52.

are much more intense than any of the others which are all converging to the $v' = 3$ vibrational level of the ion. Again, for these $v' = 3$ levels to autoionize a vibrational energy change of two quanta is necessary. This may be evidence supporting the propensity rule of Berry [35]; however, it is by no means definitive. Two lines remain unassigned as they did not fit any Rydberg series. It is quite likely that these states are being perturbed by other Rydberg states. Mischer [52] has pointed out that there is some perturbation between states with different ℓ components but the same m_ℓ quantum number.

The next vibrational step, $v' = 2$ has very little structure superimposed on it. This is probably a result of the fact that the Rydberg levels in this region must be of a very high principal quantum number and the transition probability to these states is relatively small, because of n^{-3} dependence and a small Franck-Condon factor for the $v' = 3$ level. Table XVIII presents the data on the five observed autoionization lines on this step. All of these Rydberg states are converging to $v' = 3$ as expected, since only four vibrational states were observed in the photoelectron spectrum of Turner and May [53].

It is interesting to note that if one looks in the literature only one paper may be found which mentions fine structure on the vibrational steps of NO^+ [54]. Cantone, Emma and Grasso [54] did an electron impact study of NO and a first derivative plot of their data does indeed show

some strong structure. This structure was attributed to autoionization by Cantone, et al. [54] but they did not speculate on the type of autoionization. A careful examination of the photoionization efficiency curves of Watanabe [48], Hurzeler, et al. [49] and Reese and Rosenstock [51] shows that the structure reported here is also observable in all these curves. None of these authors, however, make any mention of this structure.

The 1220 - 600 Å Region

Figure 14 is the photoionization efficiency curve for NO^+. The remaining structure between 1220 Å and 600 Å has been discussed in detail by various authors [41,55,56] in terms of Rydberg series converging to higher ionization potentials. Edquist, et al. [56] have investigated the photoelectron spectrum of NO and utilizing this information have taken all the available data on the NO spectrum and compiled it into a group of Rydberg series. Except for one difficulty most of the structure in the photoionization curve can be correlated with this compilation. Edquist, et al. [56] do not distinguish between lines reported by two different authors. For example a line reported at 800.4 Å by Tanaka [55] is assigned as the $n = 4$, $v' = 1$ member of a Rydberg series converging to 16.86 eV while a line at 800.4 Å reported by Huber [41] is assigned as $n = 3$, $v' = 0$ of a Rydberg series converging to 18.32 eV. It is obvious that this line can be only one or the other (unless

Figure 14. The photoionization efficiency curve of NO^+ from NO (1350 - 600 Å).

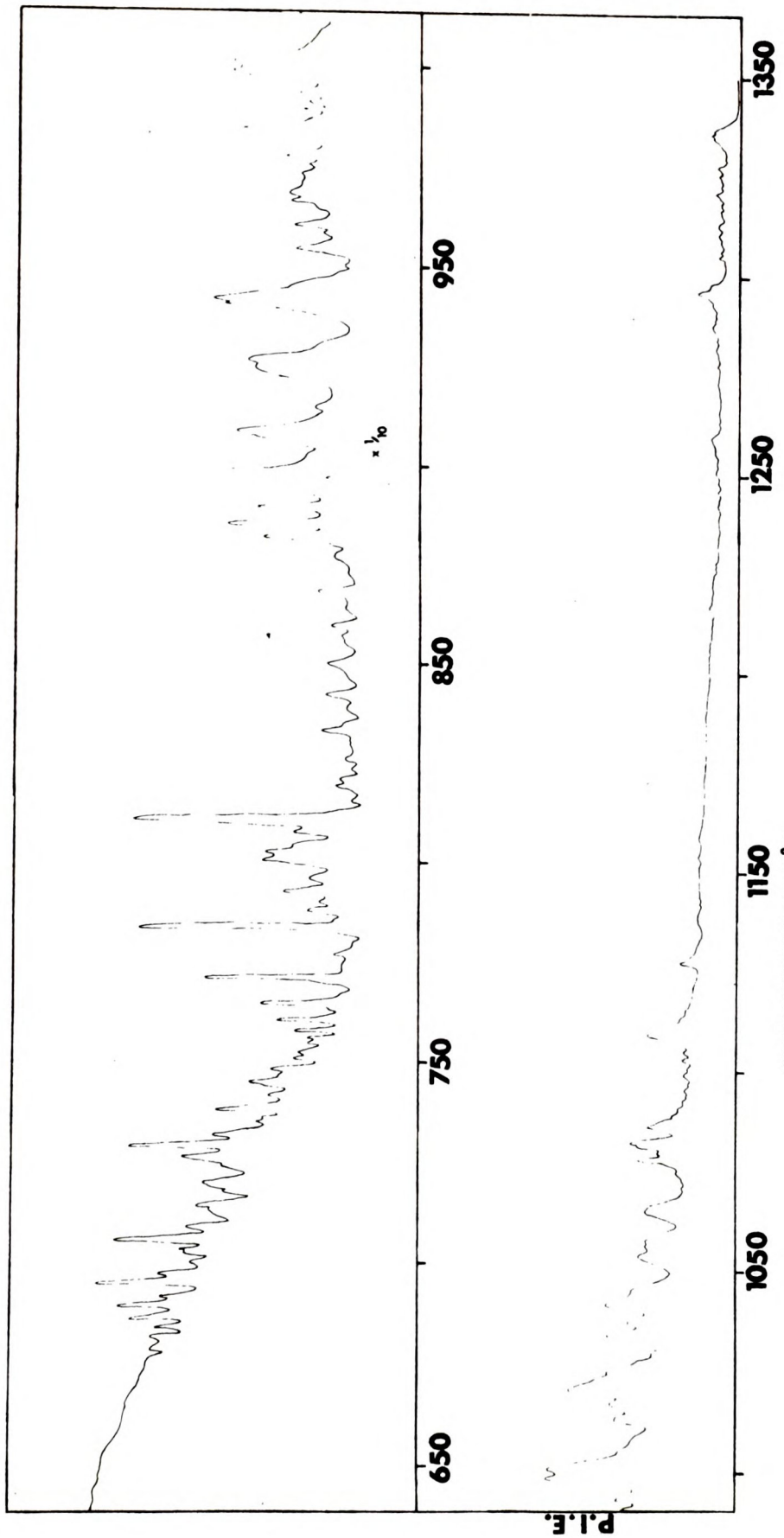

Figure 14.

superimposed). Therefore when such a controversy exists only one will be chosen.

Table XIX presents a comparison of the observed autoionization structure with that reported as belonging to an $ns\sigma$ series converging to 15.65 eV. Edquist, et al. [56] did not report any lines for the $n = 3$ member of this series. Information concerning this member of the series was obtained from the photoionization curve, the $v' = 0$ and three other vibrational components being observed.

Table XX through Table XXII present a comparison between the observed photoionization structure and the Rydberg series of Edquist, et al. [56] which converge to 16.56 eV, 16.86 eV and 17.59 eV respectively.

Table XXIII presents a comparison between the Rydberg series assigned by Edquist, et al. [56] converging to 18.07 eV and the structure in the photoionization efficiency curve. Most of the reported structure of this series has been assigned by this author to other series and it seems possible that many of the lines in this series are not resolved well enough from other lines in the spectrum. Those lines which may be unambiguously assigned to this series are listed in the Table.

Table XXIV presents the Rydberg series converging to 18.32 eV. All previously reported members of this series are observed and the series is extended to $n = 7$ with the addition of the line observed at 689.92 Å. This accounts for all the structure between 1150 Å and 600 Å.

Table XIX. A Rydberg series of NO: $1\pi \rightarrow ns\sigma(\rightarrow a^3\Sigma^+$ at 15.65 eV).

n	v'	λ_{obs}	λ_{rep} [a]	δ (calc)
3	0	1013.68		1.01
	1	993.80	$\approx$ 995.8	0.98
	2	983.30	$\approx$ 983.9	0.99
	3	973.60	$\approx$ 972.4	1.00
4	0	877.80	878.20	1.02
5	0	839.30	838.9	1.07

[a]See reference 56.

Table XX. A Rydberg series of NO: $5\sigma \rightarrow np_{\pi}^{\sigma}$ ($\rightarrow b^3\Pi$ at 16.56 eV).

n	v	λ_{obs}	λ_{rep} [a]	δ (calc)
$3p\pi$	0	897.30	897.3	0.77
	1	892.05	882.6	0.82
$3p\sigma$	0	885.55	885.4	0.70
	1	---	872.0	
$4p\pi$	0	811.05	810.9	0.63
	1	---	799.2	
$4p\sigma$	0	808.55	809.5	0.68
	1	---	797.2	
$5p_{\pi}^{\sigma}$	0	783.80	783.7	0.71
	1	771.30	772.8	0.59

[a]See reference 56.

Table XXI. A Rydberg series of NO: $1\pi \rightarrow ns\sigma$ ($\rightarrow w^3\Delta$ at 16.86 eV).

n	v	λ_{obs}	λ_{rep}[a]	δ (calc)
3	0	915.55	916.5	0.98
	1	907.55	907.4	0.99
	2	---	897.5	
	3	889.50	889.8	1.00
	4	880.55	881.8	1.01
4	0	808.55	809.5	1.02
	1	---	800.4	
	2	---	792.3	
	3	---	784.4	
	4	777.30	776.5	1.03
	5	770.05	769.7	1.03
5	0	---	775.2	
	1	765.00	767.2	0.90
	2	760.55	760.3	1.04
	3	752.80	753.3	1.05

[a]See reference 56.

Table XXII. A Rydberg series of NO: $1\pi \rightarrow ns\sigma$ ($\rightarrow b'^3\Sigma^-$ at 17.59 eV).

n	v	λ_{obs}	λ_{rep}[a]	δ (calc)
3	0	868.55	868.3	0.98
	1	860.05	859.9	0.98
	2	850.35	850.0	0.98
	3	842.55	841.7	0.98
	4	833.42	833.6	0.98
	5	826.30	825.7	0.98
	6	---	818.1	
4	3	751.30	751.0	1.04
	4	744.80	744.6	1.04
	5	738.20	738.3	1.05
	6	732.05	732.2	1.04
	7	---	726.2	
	8	---	719.2	
5	3	---	721.3	
	4	714.80	715.1	1.03
	5	709.30	709.2	1.06
	6	703.05	703.4	1.03
	7	---	697.6	

[a]See reference 56

Table XXIII. A Rydberg series of NO: $1\pi \rightarrow ns\sigma$ ($\rightarrow W'^1\Delta$ at 18.07 eV).

n	v	λ_{obs}	λ_{rep}[a]	δ (calc)
3	1	---	830.0	
	2	821.30	821.0	0.96
	3	812.80	812.7	0.96
	4	804.55	804.9	0.96
	5	796.30	795.8	0.95
	6	787.30	787.1	0.93

[a]See reference 56.

Table XXIV. A Rydberg series of NO: $5\sigma \rightarrow np^{\sigma}_{\pi}$ ($\rightarrow A'^{2}\Pi$ at 18.32 eV).

n	v	λ_{obs}	λ_{rep}[a]	δ (calc)
$3p\pi$	0	800.80	800.40	0.81
	1	790.30	789.8	0.81
$3p\sigma$	0	793.05	793.0	0.75
	1	783.20	---	0.75
$4p\pi$	0	729.30	728.9	0.79
	1	720.30	720.3	0.78
$4p\sigma$	0	726.55	726.7	0.72
	1	718.05	717.8	0.70
5p	0	706.05	706.0	0.77
	1	697.80	697.6	0.74
6p	0	695.55	695.4	0.78
	1	687.55	---	0.73
7p	0	698.92	---	0.77

[a]See reference 56.

Between 1220 Å and 1150 Å there are eighteen lines. Reese and Rosenstock [51] reported fifteen lines in this region and placed eight of them into two progressions. However, two of their fifteen lines are not observed in this study. The reason for this is not clear since both experiments should have yielded the same results. Possibly some artifact was introduced into the experiment of Reese and Rosenstock [51]. Eight of the peaks in this region may still be placed into two progressions as follows: (a) 1077.93 Å, 1064.93 Å, 1053.55 Å, and 1041.80 Å; (b) 1056.66 Å, 1044.80 Å, 1033.68 Å, and 1024.93 Å. The remainder of the structure is not accounted for and may belong to the autoionization of non-Rydberg type transitions. The eighteen lines observed are listed in Table XXV.

In conclusion the autoionization structure in the threshold region has been assigned as vibrational autoionization, and the structure in the remaining portion of the photoionization efficiency curve has been correlated with the proposed Rydberg series of Edquist, et al. [56].

Table XXV. Unassigned autoionization structure in NO.

λ_{obs}
1128.56
1110.31
1086.56
1082.18
1077.93
1064.93
1056.68
1053.55
1044.80
1041.80
1037.18
1033.68
1024.93
1020.68
1017.18
1001.80

REFERENCES

REFERENCES

1. E. Wigner, Phys. Rev. 73, 1002 (1948).

2. G. H. Wannier, Phys. Rev. 90, 817 (1953).

3. S. Geltman, Phys. Rev. 102, 171 (1956).

4. A. J. C. Nicholson, J. Chem. Phys. 39, 954 (1963).

5. J. A. R. Samson, Techniques of Vacuum Ultraviolet Spectroscopy, John Wiley and Sons: New York, 1967 .

6. J. Berkowitz and W. A. Chupka, J. Chem. Phys. 45, 1287 (1966).

7. W. A. Chupka and J. Berkowitz, J. Chem. Phys. 47, 4320 (1967).

8. R. Allison, J. Burns and A. J. Tuzzolino, J. Opt. Soc. Am. 54, 747 (1964).

9. G. V. Marr, Photoionization Processes in Gases, Academic Press: New York, 1967.

10. W. A. Chupka and J. Berkowitz, J. Chem. Phys. 47, 2921 (1967).

11. T. Nakayama, M. Y. Kitamura, and K. Watanabe, J. Chem. Phys. 30, 1180 (1959).

12. C. R. Brundle, Chem. Phys. Letters 5, 410 (1970); C. R. Brundle, D. Neumann, W. C. Price, D. Evans, A. W. Potts, and D. G. Streets, J. Chem. Phys. 53, 705 (1970).

13. Later measurements indicate NO_2 introduced pure but breaks down (by reaction with hot mercury in the pumps, etc.) to give NO which is not pumped rapidly, W. A. Chupka, Private Communication.

14. W. C. Price and D. M. Simpson, Trans. Far. Soc. 37, 106 (1941).

15. Y. Tanaka and A. S. Jursa, J. Chem. Phys. 36, 2493 (1962).

16. J. Collin and F. P. Lossing, J. Chem. Phys. 28, 900 (1958).

17. R. J. Kandell, J. Chem. Phys. 23, 84 (1955).

18. S. Tsuda and W. H. Hamill, Adv. Mass Spectry. 3, 249 (1966).

19. R. W. Kiser and I. C. Hisatsune, J. Phys. Chem. 65, 1444 (1961).

20. E. C. G. Stuecklberg and H. D. Smyth, Phys. Rev. 36, 478 (1930).

21. P. Natalis and J. E. Collin, Chem. Phys. Letters 2, 79 (1968).

22. O. Edquist, E. Lindholm, L. E. Selin, L. Asbrink, C. E. Kuyatt, S. R. Mielczarek, J. A. Simpson and I. Fischer-Hjalmers, Physica Scripta 1, 172 (1970).

23. V. H. Dibeler, J. A. Walker and S. K. Liston, J. Res. Natl. Bur. Std. 71a, 371 (1967).

24. D. C. Frost, D. Mak and C. A. McDowell, Can. J. Chem. 40, 1064 (1962).

25. G. L. Weissler, J. A. R. Samson, M. Ogawa and G. R. Cook, J. Opt. Soc. Am. 49, 338 (1959).

26. R. S. Mulliken, J. Chem. Phys. 3, 720 (1935).

27. A. D. Walsh, J. Chem. Soc., 2266 (1953).

28. L. Harris and G. W. King, J. Chem. Phys. 8, 775 (1940).

29. S. Claesson, J. Donohue and V. Schomaker, J. Chem. Phys. 16, 207 (1948).

30. G. Herzberg, Electronic Spectra and Electronic Structure of Molecules, Van Nostrand: New Jersey, 1967.

31. J. N. Bardsley, Chem. Phys. Letters 2, 329 (1968).

32. G. Herzberg, Spectra of Diatomic Molecules, Van Nostrand: New Jersey, 1950.

33. U. Fano, Phys. Rev. 124, 1866 (1961).

34. U. Fano and J. W. Cooper, Rev. Mod. Phys. 40, 441 (1968).

35. R. S. Berry, J. Chem. Phys. 45, 1228 (1966).

36. P. Natalis, J. Delwiche and J. E. Collin, Chem. Phys. Letters 9, 139 (1971).

37. F. C. Fehsenfeld, E. E. Ferguson and M. Mosesman, Chem. Phys. Letters 4, 73 (1969).

38. J. L. Franklin, J. G. Dillard, H. M. Rosenstock, J. T. Herron, K. Draxl and F. H. Field, Ionization Potentials, Appearance Potentials, and Heats of Formation of Gaseous Positive Ions, (NSRDS-NBS 26, 1969).

39. Victor Fong, Masters Thesis, Michigan State University (1970).

40. P. Gray and A. Williams, Chem. Rev. 59, 239 (1959).

41. K. P. Huber, Helv. Phys. Acta 34, 929 (1961).

42. JANAF Thermochemical Tables (Dow Chemical Company, Clearinghouse for Federal Scientific and Technical Information, Springfield, Va., 1967).

43. C. E. Moore, Ionization Potentials and Ionization Limits Derived from the Analysis of Optical Spectra, (NSRDS-NBS 34, 1970).

44. A. S. Newton and A. F. Sciamanna, J. Chem. Phys. 44, 4327 (1966).

45. A. S. Newton and A. F. Sciamanna, J. Chem. Phys. 52, 327 (1970).

46. A. B. F. Duncan, Rydberg Series in Atoms and Molecules, Academic Press: New York, 1971.

47. K. Watanabe, F. F. Marmo and E. C. Y. Inn, Phys. Rev. 91, 1155 (1953).

48. K. Watanabe, J. Chem. Phys. 22, 1564 (1954).

49. H. Hurzeler, M. G. Inghram and J. D. Morrison, J. Chem. Phys. 28, 76 (1958).

50. A. J. C. Nicholson, J. Chem. Phys. 43, 1171 (1965).

51. R. M. Reese and H. M. Rosenstock, J. Chem. Phys. 44, 2007 (1966).

52. E. Miescher, J. Mol. Spectry. 20, 130 (1966).

53. D. W. Turner and D. P. May, J. Chem. Phys. 45, 471 (1966).

54. B. Cantone, V. Emma and F. Grasso, in Advances in Mass Spectrometry, E. Kendrik, Editor, The Institute of Petroleum: London, 1968. Vol. IV, p. 599.

55. Y. Tanaka, Sci. Papers. Inst. Phys. Chem. Res. (Tokyo) 39, 456 (1942).

56. O. Edquist, E. Lindholm, L. E. Selin, H. Sjörgen and L. Asbrink, Arkiv Fysik 40, 439 (1970).